

# A Short Lecture on Topological Crystallography and a Discrete Surface Theory

Hisashi NAITO

Graduate School of Mathematics, Nagoya University, Nagoya 464-8602, JAPAN  
naito@math.nagoya-u.ac.jp

## Abstract

In this note, we discuss topological crystallography, which is a mathematical theory of crystal structures. The most symmetric structure among all placements of the graph is obtained by a variational principle in topological crystallography. We also discuss a theory of trivalent discrete surfaces in 3-dimensional Euclidean space, which are mathematical models of crystal/molecular structures.

## 1 Introduction

Geometric analysis is a field of analysis on geometric objects such as manifolds, surfaces, and metric spaces. Discrete geometric analysis is an analysis on *discrete* geometric objects, for example, graphs, and contains the spectral theory and the probability theory of graphs. Topological crystallography and a discrete surface theory based on crystal/molecular structures are also parts of discrete geometric analysis.

Topological crystallography is a mathematical theory of crystal structures, which is founded by M. Kotani and T. Sunada [20, 21, 22, 39]. In physics, chemistry, and mathematics, crystal structures are described by space groups, which denote symmetry of placements of atoms. The usual description of crystals contains bonds between atoms in crystals. However, space groups do not consider such atomic bonds. Graphs are also natural notions to describe crystal structure, since vertices and edges of graphs correspond to atoms and atomic bonds in crystals, respectively. On the other hand, one of the important notions of physical phenomena is the principle of the least action, which corresponds to the variational principle in mathematics. That is to say, to describe physical phenomena, first we define an energy functional, which is called a Lagrangian in physics, and then we may find such phenomena as minimizers of the energy functional. There is no direct relationship between descriptions of crystal structures by using space groups and the principle of the least action.

Topological crystallography gives us a direct relationship between symmetry of crystal structures and the variational principle. Precisely, for a given graph structure which describes a crystal, we define the energy of realizations of the graph (placements of vertices of the graph in suitable dimensional Euclidean space), and obtain a “good” structure as a minimizer of the energy. Moreover, such structures give us most symmetric among all placements of the graph, which is proved by using the theory of random walk on graphs.

Molecular structures can be also described by using graph theory. The Hückel molecular orbital method, which is an important theory in physical chemistry, and the tight binding approximation for studying electronic states of crystals can be regarded as spectral theories of graphs from mathematical viewpoints. In this way, discrete geometric analysis can be applied to physics, chemistry, and related technologies.

In the first few sections, we discuss topological crystallography including graph theory and geometry. The most important bibliography of this part is T. Sunada’s lecture note [38]. The author discusses an introduction to topological crystallography along with it.

On the other hand, we can regard some of crystal/molecular structures, for example, fullerenes and carbon nanotubes (see Section 3.3), as surfaces, especially, as discrete surfaces. Recently,  $sp^2$ -carbon structures (including fullerenes and nanotubes) are paid attention to in sciences and technologies, since they have rich  $\pi$ -electrons and hence rich physical properties. In mathematical words,  $sp^2$ -carbon structures can be regarded as trivalent graphs in  $\mathbb{R}^3$ , and hence trivalent *discrete surfaces*. There are many discrete surface theories in mathematics, but they are discretization or discrete analogue of continuous/smooth objects. For example, discrete surfaces of triangulations are used in computer graphics, which is a discretization of smooth real objects. In other words, conventional discrete surface theories are “from continuous to discrete”. In contrast, discrete surfaces, which describe crystal/molecular structures, are essentially discrete. Even for the case of trivalent discrete surfaces, it is not easy to define curvatures of them.

In the last few sections, we discuss a theory of trivalent discrete surfaces in  $\mathbb{R}^3$ , and also discuss subdivisions/convergences of them. Hence, our discrete surface theory is “from discrete to continuous”.

## 2 Preliminaries

### 2.1 Graph theory

Here, we prepare a graph theory to describe topological crystals and discrete surfaces. Definitions and notations are followed by standard text books of graph theory, for example [3, 5].

**Definition 2.1.** An ordered pair  $X = (V, E)$  is called a *graph*, if  $V$  is a countable set and  $E = \{(u, v) : u, v \in V\}$ . An element  $v \in V$  is called a vertex of  $X$ , and an element  $e \in E$  is called an edge of  $X$ . For each element  $e = (u, v) \in E$ , we may also write  $u = o(e)$  and  $v = t(e)$ , which are called the *origin* and the *terminus* of  $e$ .

**Definition 2.2.** A graph  $X = (V, E)$  is called *finite*, if the number of vertices  $|V|$  and the number of edges  $|E|$  are finite.

For a vertex  $v \in V$ , write  $E_v = \{(v, u) \in E\}$ , which is the set of edges with  $o(e) = v$ . The number of edges emanating with  $v \in V$  is called the *degree*  $\deg(v) = |E_v|$  of  $v$ . If  $\deg(v)$  is finite for any  $v \in V$ , then the graph  $X$  is called *locally finite*. For any  $e = (u, v) \in E$ ,  $\bar{e} = (v, u) \in E$ , then  $X$  is called *non-oriented*, otherwise  $X$  is called *oriented*.

In this note, we only consider non-oriented and locally finite graphs. Moreover, we admit graphs which contain a loop  $(u, u) \in E$  and multiple edges.

**Definition 2.3.** For a graph  $X = (V, E)$ , successive edges  $(u_1, u_2)(u_2, u_3) \cdots (u_{k-2}, u_{k-1})(u_{k-1}, u_k)$ , where  $(u_i, u_j) \in E$ , is called a *path* between  $u_1$  and  $u_k$ , and if  $u_1 = u_k$  and the path does not contain backtracking edges, it is called a *closed path*. A graph is *connected*, if there exists a path between arbitrary two vertices. A connected graph is called *tree*, if the graph contains no closed path.

**Example 2.4.** Both graphs in Fig. 2.1 are the same as each other, and are called  $K_4$  graph. Each vertex of  $K_4$  graph is connected with all of the other vertices. A graph with such a property is called a *complete graph*. The  $K_4$  graph is the complete graph with 4 vertices.

**Definition 2.5.** Let  $X = (V, E)$  be a finite graph with  $V = \{v_i\}_{i=1}^n$ . The *adjacency matrix*  $A = A_X$  of  $X$  is an  $n \times n$  matrix defined by  $a_{ij}$  = number of edges  $(v_i, v_j)$ .

If a graph  $X$  is non-oriented, then the adjacency matrix of  $X$  is symmetric.

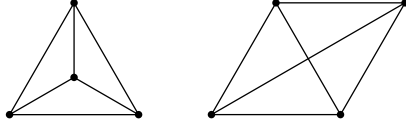


Figure 2.1:  $K_4$  graph, each is different figure of the same graph.

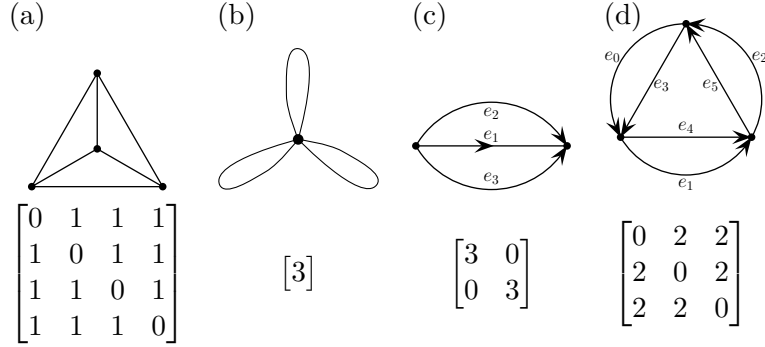


Figure 2.2: Examples of graphs and their adjacency matrices.

**Remark 2.6.** Let  $A$  be an adjacency matrix of a graph  $X$ ,

1.  $(i, j)$ -element of  $A^k$  expresses number of paths from  $v_i$  to  $v_j$  by  $k$ -steps
2. if  $A^{n-1}$  ( $n = |V|$ ) is not block diagonal, then  $X$  is connected
3. if  $X$  is simple and non-oriented, then  $(1/6) \text{tr}(A^3)$  expresses the number of triangles contained in  $X$

**Definition 2.7.** Let  $X = (V, E)$  be a finite non-oriented graph. A tree  $X_1 = (V, E_1)$  is called a *spanning tree* of  $X$ , if it satisfies  $E_1 \subset E$  and for any  $e \in E \setminus E_1$ ,  $(V, E_1 \cup \{e\})$  contains a closed path (see Fig. 2.3).



Figure 2.3: Each graph is a spanning tree of  $K_4$  graph.

Now, we also consider homology groups of graphs. A graph  $X = (V, E)$  can be considered as a 1-dimensional CW complex as follows: the 0-dimensional chain group  $C_0$  is the  $\mathbb{Z}$ -module consisted by  $V$ , and the 1-dimensional chain group  $C_1$  is the  $\mathbb{Z}$ -module consisted by  $E$ . The boundary operator  $\partial: C_1 \rightarrow C_0$  is defined by

$$\partial(e) = t(e) - o(e),$$

where  $o(e)$  and  $t(e)$  are the origin and terminus of the edge  $e$ , namely,  $o(e) = u$  and  $t(e) = v$ , if  $e = (u, v)$ . The homology group  $H_0(X, \mathbb{Z})$  and  $H_1(X, \mathbb{Z})$  is defined by

$$H_1(X, \mathbb{Z}) = \ker \partial \subset C_1(X), \quad H_0(X, \mathbb{Z}) = C_0(X) / \text{image } \partial.$$

The following proposition explains particular properties for the first homology group on graphs.

**Proposition 2.8** (Sunada [39]). *Let  $X = (V, E)$  be a locally finite graph. Then, any non-trivial closed path  $e$  satisfies  $[e] \neq [0] \in H_1(X, \mathbb{Z})$ . Conversely, for each non-zero element  $h \in H_1(X, \mathbb{Z})$ , there exists a closed path  $e$  in  $X$  such that  $h = [e]$ .*

*Proof.* Let  $e = e_1 \cdots e_k$  ( $e_i \in E$ ) a path in  $X$ . Then, we may write  $e = e_1 + \cdots + e_k \in C_1(X, \mathbb{Z})$ , and  $\partial(e) = t(e_1) - o(e_1) + t(e_2) - o(e_2) + \cdots + t(e_k) - o(e_k)$ . Since  $o(e_{i+1}) = t(e_i)$ , we obtain  $\partial(e) = t(e_1) - o(e_k)$ . Assuming  $e$  is closed, that is  $o(e_1) = t(e_k)$ , we obtain  $\partial(e) = 0$ , and  $[e] \neq [0] \in H_1(X, \mathbb{Z})$ .

Conversely, we take an  $h \in H_1(X, \mathbb{Z}) = \ker \partial \subset C_1(X, \mathbb{Z})$ , and let  $C_1(X) = \text{span}\{e_i : i = 1, \dots, n\}$ , then there exists  $\alpha_i \in \mathbb{Z}$  such that  $h = \alpha_1 e_1 + \cdots + \alpha_n e_n$ , and  $\partial h = 0$ . The equation  $\partial h = \sum \alpha_i (t(e_i) - o(e_i))$  implies  $h$  is the sum of closed paths (see [38, p.41]).  $\square$

Proposition 2.8 implies that an elements of  $H_1(X, \mathbb{Z})$  corresponds to a closed path of  $X$ . Hence we obtain a method for counting the rank of  $H_1(X, \mathbb{Z})$ .

**Proposition 2.9.** *Let  $X = (V, E)$  be a finite non-oriented graph, and  $X_1 = (V, E_1)$  be a spanning tree of  $X$ . Then, the first homology group  $H_1(X, \mathbb{Z})$  of  $X$  satisfies  $\text{rank } H_1(X, \mathbb{Z}) = |E| - |E_1|$ .*

*Proof.* Since  $X_1$  is a tree,  $X_1$  does not contain closed path. For each edge  $e_0 = (u, v) \in E \setminus E_1$ , we may find unique path  $e = e_1 \cdots e_k$  in  $X_1$  with  $o(e_1) = v$ ,  $t(e_k) = u$ , and hence,  $\tilde{e}_0 = e_0 e$  is a closed path in  $X$ . By Proposition 2.8, we obtain  $[\tilde{e}_0] \in H_1(X, \mathbb{Z})$ . Therefore, for each  $e_i \in E \setminus E_1$ , there exists  $[\tilde{e}_i] \in H_1(X, \mathbb{Z})$  by a similar manner, and  $\{[\tilde{e}_i]\}$  are linearly independent.  $\square$

**Example 2.10.** The rank of the first homology group of graphs in Fig. 2.2 are (a) 3, (b) 3, (c) 2, and (d) 4, respectively.

**Remark 2.11.** An algorithm to find a spanning tree of a finite graph is well-known as Kruskal's algorithm, which finds a spanning tree within  $O(|E| \log |E|)$  (see for example [1]).

## 2.2 Covering spaces

Definitions and notations are followed by standard text books of geometry and topology, for example [36].

**Definition 2.12.** Let  $X$  and  $X_0$  be topological spaces. The space  $X$  is a *covering space* of  $X_0$  if there exists a surjective continuous map  $p: X \rightarrow X_0$ , which is called a *covering map*, such that for each  $x \in X_0$ , there exists an open neighbourhood  $U$  of  $x$  and open sets  $\{V_i\} \subset X$  satisfying  $p^{-1}(U) = \sqcup V_i$  with  $p|_{V_i}: V_i \rightarrow U$  homeomorphic.

**Theorem 2.13.**

1. For any topological space  $X_0$ , there exists the unique simply connected covering space  $\tilde{X}$ , which is called the universal covering of  $X_0$ .
2. If  $p: X \rightarrow X_0$  is a covering map, then there exists a transformation group  $T$  on  $X$  such that for any  $\sigma \in T$ ,  $p \circ \sigma = p$ . The group  $T$  is called the covering transformation group.
3. The covering transformation group of  $p: \tilde{X} \rightarrow X_0$  is the fundamental group  $\pi_1(X)$  of  $X$ .

$$\begin{array}{ccccc}
 & & p \circ q & & \\
 & & \downarrow & & \downarrow \\
 & & \text{covering} & & \\
 \tilde{X} & \xrightarrow{q} & X & \xrightarrow{p} & X_0 \\
 & \text{covering} & & \text{covering} & \\
 \{e\} & \xleftarrow{q_*} & \pi_1(X) & \xleftarrow{p_*} & \pi_1(X_0) \\
 & \text{hom.} & & \text{hom.} & \\
 & & q_* \circ p_* & & \\
 & & \uparrow & & \uparrow \\
 & & \text{hom.} & & 
 \end{array}$$

**Example 2.14.**

1. The real line  $\mathbb{R}$  is a covering space of  $S^1$ , since  $p: \mathbb{R} \rightarrow S^1, p(x) = x \pmod{2\pi}$ . Since  $\mathbb{R}$  is simply connected and the covering transformation group of  $p$  is  $\mathbb{Z}$ , we obtain  $\pi_1(S^1) \cong \mathbb{Z}$ .
2. The 2-dimensional Euclidean space  $\mathbb{R}^2$  is a covering space of  $T^2 = \mathbb{R}^2/\mathbb{Z}^2$ , since  $p: \mathbb{R}^2 \rightarrow T^2, p(x, y) = (x \pmod{2\pi}, y \pmod{2\pi})$ . Since  $\mathbb{R}^2$  is simply connected and the covering transformation group of  $p$  is  $\mathbb{Z}^2$ , we obtain  $\pi_1(T^2) \cong \mathbb{Z}^2$ .

**Definition 2.15** (Sunada [39]). A covering  $p: X \rightarrow X_0$  with an abelian covering transformation group is called an *abelian covering*. For any topological space  $X_0$ , there exists a *maximal abelian covering* space  $X$ , since  $H_1(X_0, \mathbb{Z}) = \pi_1(X_0)/[\pi_1(X_0), \pi_1(X_0)]$  is a maximal abelian subgroup of  $\pi_1(X_0)$

**Example 2.16.** The universal covering graph of the 3-bouquet graph  $X$  (Fig. 2.2 (b)) is a tree graph with the degree 3. The fundamental group  $\pi_1(X)$  is the free group with 3 elements, and the first homology group  $H_1(X, \mathbb{Z})$  is  $\mathbb{Z}^3$ . For any normal subgroup  $S \subset H_1(X, \mathbb{Z})$ , there exists a graph  $X_S$  such that  $X_S$  is a covering graph of  $X$  with its covering transformation group  $S$ .

### 3 Topological crystals and their standard realization

The classical description of crystallography is based on group theory, and they describe symmetries of crystals. For example, in the classical crystallography, the diamond crystal is classified as the space group  $Fd\bar{3}m$  (see Section A.1), and the group does not contain information of chemical bonds of atoms in the crystal.

The theory of topological crystals is developed by Kotani–Sunada [18, 20, 21, 22]. The theory describes symmetries of crystals including chemical bonds of atoms, and it is based on variational problems.

#### 3.1 Topological crystals and their realizations

In this section, we assume that graphs are connected non-oriented locally finite, which may include self-loops and multiple edges.

**Definition 3.1** (Sunada [39]). A connected non-oriented locally finite graph  $X = (V, E)$ , which may include self-loops and multiple edges, is called a *topological crystal* (or a *crystal lattice*), if and only if there exists an abelian group  $G$  which acts freely on  $X$ . The topological crystal is *d-dimensional* if the rank of the abelian group  $G$  is  $d$ .

By this definition, for a topological crystal  $X = (V, E)$ , there exists a finite graph  $X_0 = (V_0, E_0)$  satisfying  $X/G = X_0$ , for an abelian subgroup  $G \subset H_1(X_0, \mathbb{Z})$ , and  $X$  is a covering graph of  $X_0$  whose covering transformation group is  $G$ . On the contrary, for a given connected non-oriented finite graph  $X_0 = (V_0, E_0)$  and an abelian subgroup  $G \subset H_1(X_0, \mathbb{Z})$ , there exists a topological crystal  $X$  with  $X/G = X_0$ , by taking a suitable covering graph.

**Definition 3.2** (Sunada [39]). A topological crystal  $X$  is called *maximal abelian* if and only if  $G = H_1(X_0, \mathbb{Z})$ .

**Example 3.3.** A square lattice  $X$  (Fig. 3.1 (a)) is a topological crystal whose base graph  $X_0$  is the graph in Fig. 3.3 (a) (the 2-bouquet graph). Since the covering transformation group  $G$  is  $G = H_1(X_0, \mathbb{Z})$  and  $\text{rank } G = \text{rank } H_1(X_0, \mathbb{Z}) = 2$ , the topological crystal  $X$  is 2-dimensional and maximal abelian.

**Example 3.4.** A triangular lattice  $X$  (Fig. 3.1 (b)) is a topological crystal whose base graph  $X_0$  is the graph in Fig. 2.2 (b). Since the covering transformation group  $G$  satisfies  $\text{rank } G = 2$  but  $H_1(X_0, \mathbb{Z}) = 3$ , the topological crystal  $X$  is 2-dimensional and not maximal abelian.

**Example 3.5.** A hexagonal lattice  $X$  (Fig. 3.1 (c)) is a topological crystal whose base graph  $X_0$  is the graph in Fig. 2.2 (c). Since the covering transformation group  $G$  is  $G = H_1(X_0, \mathbb{Z})$  and  $\text{rank } G = \text{rank } H_1(X_0, \mathbb{Z}) = 2$ , the topological crystal  $X$  is 2-dimensional and maximal abelian.

**Example 3.6.** A kagome lattice  $X$  (Fig. 3.1 (d)) is a topological crystal whose base graph  $X_0$  is the graph in Fig. 2.2 (d). Since the covering transformation group  $G$  satisfies  $\text{rank } G = 2$  but  $H_1(X_0, \mathbb{Z}) = 4$ , the topological crystal  $X$  is 2-dimensional and not maximal abelian.

**Example 3.7.** A diamond lattice  $X$  (Fig. 3.19) is a topological crystal whose base graph  $X_0$  is the graph in Fig. 2.2 (b) (the 3-bouquet graph). Since the covering transformation group  $G$  is  $G = H_1(X_0, \mathbb{Z})$  and  $\text{rank } G = \text{rank } H_1(X_0, \mathbb{Z}) = 3$ , the topological crystal  $X$  is 3-dimensional and maximal abelian.

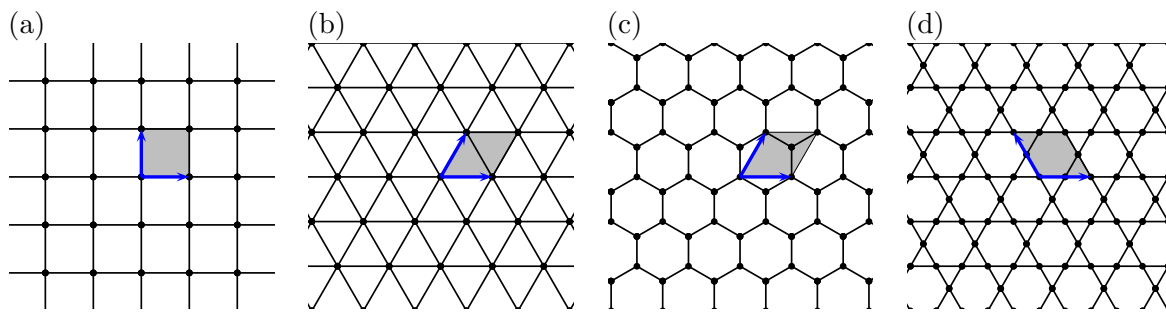


Figure 3.1: Standard realizations of representative 2-dimensional topological crystals. (a) A square lattice, (b) a triangular lattice, (c) a hexagonal lattice, and (d) a kagome lattice. Blue vectors are basis of parallel translations.

**Definition 3.8** (Sunada [39]). Given  $d$ -dimensional topological crystal  $X = (V, E)$ , a piecewise linear map  $\Phi: X \rightarrow \mathbb{R}^d$  is called a *realization* of  $X$ . More precisely, first we define  $\Phi: V \rightarrow \mathbb{R}^d$ , and define  $\Phi(e)$  by linear interpolation between  $\Phi(o(e))$  and  $\Phi(t(e))$ .

**Definition 3.9** (Sunada [39]). A realization  $\Phi$  of a  $d$ -dimensional topological crystal  $X$  is called a *periodic realization*, if there exists an injective homomorphism  $\rho: G \rightarrow \mathbb{R}^d$  satisfying

$$\Phi(gv) = \Phi(v) + \rho(g), \quad (v \in V, g \in G).$$

**Example 3.10.** Three realizations in Fig. 3.2 are periodic realizations of a hexagonal lattice. These are different periodic realizations of the same graph. The realization (b) is the most symmetric, and the main problem of this section is to explain the reason why nature selects (b) by mathematics.

**Definition 3.11** (Sunada [39]). Let  $X$  be a  $d$ -dimensional topological crystal with the base graph  $X_0 = (V_0, E_0)$ ,  $G$  be an abelian group acting on  $X$ , and  $\Phi$  or  $(\Phi, \rho)$  be a periodic realization of  $X$ , where  $\rho: G \rightarrow GL(d, \mathbb{R})$ . The *energy* and the *normalized energy* of  $\Phi$  are defined by

$$E(\Phi) = \sum_{e \in E_0} |\Phi(t(e)) - \Phi(o(e))|^2, \quad (3.1)$$

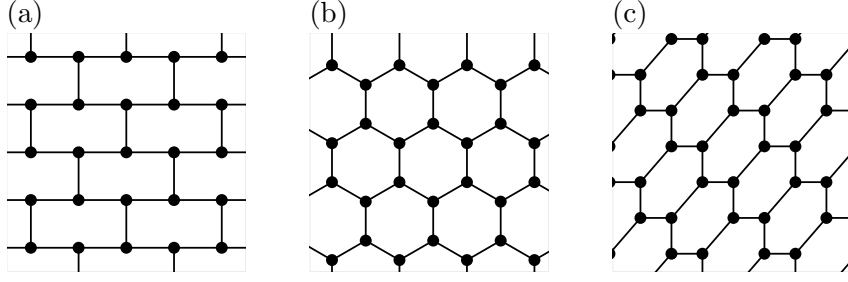


Figure 3.2: Different realizations of the hexagonal lattice. These three lattices have the same topological structure.

and

$$E(\Phi, \rho) = \text{Vol}(\Gamma)^{2/d} \sum_{e \in E_0} |\Phi(t(e)) - \Phi(o(e))|^2, \quad \Gamma = \rho(G), \quad (3.2)$$

respectively.

The energy of  $\Phi$  is a discrete analogue of the Dirichlet energy for smooth maps, since  $\Phi(t(e)) - \Phi(o(e))$  is a discretization of differential of smooth maps.

**Definition 3.12** (Sunada [39]). For a topological crystal  $X$  with fixed lattice  $\Gamma = \rho(G)$ , a critical point  $\Phi$  of the energy  $E$  is called a *harmonic realization* of  $X$ .

In the followings, we abbreviate  $\mathbf{v} = \Phi(v)$  and  $\mathbf{e} = \Phi(e)$  for  $v \in V$  and  $e \in E$ , as long as there are no misunderstandings.

**Proposition 3.13** (Sunada [39]). For a topological crystal  $X$ , a realization  $\Phi$  is harmonic if and only if

$$\sum_{(u,v) \in (E_0)_v} (\mathbf{u} - \mathbf{v}) = \mathbf{0}, \quad \text{for all } v \in V_0. \quad (3.3)$$

That is to say, the sum of vectors creating edges emanating from each  $v$  is zero, in other words, each vertex of  $V$  satisfies the “balancing condition”.

*Proof.* First, we note that we have  $E(\Phi) = E(\Phi, \rho)$  by fixing  $\Gamma$  with  $\text{Vol}(\Gamma) = 1$ . Let  $\Phi_t: X \rightarrow \mathbb{R}^d$  be a variation of  $\Phi$  with  $\Phi_0 = \Phi$ . Differentiating  $E(\Phi_t)$  by  $t$  and using the “integration by parts”, we may calculate as

$$\frac{d}{dt} E(\Phi_t) = \sum_{v \in V_0} \sum_{u \in V_v} \langle \mathbf{v}(t) - \mathbf{u}(t), \mathbf{v}'(t) - \mathbf{u}'(t) \rangle = 2 \sum_{v \in V_0} \sum_{u \in V_v} \langle \mathbf{v}(t) - \mathbf{u}(t), \mathbf{u}'(t) \rangle,$$

where  $\mathbf{v}(t) = \Phi_t(v)$  and  $\mathbf{v}'(t) = \frac{d}{dt} \Phi_t(v)$ . Therefore, we obtain

$$\left. \frac{d}{dt} E(\Phi_t) \right|_{t=0} = 2 \sum_{v \in V_0} \sum_{u \in V_v} \langle \mathbf{v} - \mathbf{u}, \mathbf{x}_u \rangle, \quad \mathbf{x}_u = \Phi'_t(u)|_{t=0},$$

and get the result. □

**Remark 3.14.**

1. In the Definition 3.12, if we do not assume that the lattice  $\Gamma$  is fixed, then critical points admit  $\Phi = 0$ .

2. The equation (3.3) is equivalent to a linear equation

$$\begin{aligned} -\deg(v)\mathbf{v} + \sum_{u \in (V_0)_v} \mathbf{u} &= 0, \quad \text{for all } v \in V_0, \\ \Delta_X \Phi &= 0, \end{aligned} \tag{3.4}$$

where  $\Delta_X = A_X - \text{diag}(\deg(v))$  and is called the *Laplacian* of  $X$ .

For a smooth map  $u: \Omega \rightarrow \mathbb{R}$  with  $u|_{\partial\Omega} = 0$ , where  $\Omega$  is a domain in  $\mathbb{R}^N$ , the Dirichlet energy  $E$  of  $u$  is defined by  $E(u) = \frac{1}{2} \int_{\Omega} |\nabla u|^2 dV$ , and its Euler-Lagrange equation is  $\Delta u = 0$  (the Laplace equation). This is a reason why the critical points of  $E$  for topological crystals are called harmonic.

**Example 3.15.** Realizations (b) and (c) of Fig. 3.2 are harmonic, since each vertex  $v \in V_0$  satisfies the balance condition (3.4), but the realization (a) of Fig. 3.2 is not harmonic. Hence, the harmonic condition (3.3) or (3.4) are not suffice to select (b) among three realizations in Fig. 3.2.

**Proposition 3.16** (Sunada [39]). *Harmonic realizations of  $X$  are unique up to affine transformations.*

*Proof.* First, note that the equation (3.3) is invariant under affine transformations. Let  $\{e_i\}_{i=1}^d$  be a  $\mathbb{Z}$ -basis of the abelian group  $G$ , which acts on  $X$ . Assume  $\Phi_1(X)$  and  $\Phi_2(X)$  are harmonic realizations of  $X$  with respect to lattice  $\Gamma_1 = \rho_1(L)$  and  $\Gamma_2 = \rho_2(L)$ , respectively. Then, there exists an  $A \in GL(d, \mathbb{R})$  such that  $\rho_1(g) = A\rho_2(g)$  for  $g \in G$ . Hence, we obtain that there exists  $\mathbf{b} \in \mathbb{R}^d$  such that  $\Phi_1 = A\Phi_2 + \mathbf{b}$ .  $\square$

**Definition 3.17** (Sunada [39]). For a topological crystal  $X$ , *standard* realizations of  $X$  are critical points among all realization  $\Phi$  and  $\Gamma$  with  $\text{Vol}(\Gamma) = 1$ .

A Standard realization are also called an *equilibrium placement* defined by Delgado-Friedrichs–O’Keeffe [6].

**Theorem 3.18** (Kotani–Sunada [21], Sunada [39]). *For any topological crystals  $X$ , there exists the unique standard realization up to Euclidean motions.*

Kotani–Sunada proved Theorem 3.18 by using a theory of harmonic maps. Eells–Sampson [9] proved the existence theorem of harmonic maps from compact Riemannian manifolds into non-positively curved Riemannian manifolds. The energy (3.1) is the Dirichlet energy of maps from 1-dimensional CW complex into a Euclidean space. Hence, by Eells–Sampson’s theorem, there exists a standard realization (an energy minimizing harmonic map) in each homotopy class. Sunada also gave another proof of Theorem 3.18 in his lecture note [39]. On the other hand, the existence of standard realizations can be also proved by showing the strong convexity of the energy (3.1).

**Theorem 3.19** (Sunada [37, 38, 39]). *For a  $d$ -dimensional topological crystal  $X$ , a realization  $\Phi$  is standard if and only if*

$$\sum_{e \in E_0} \mathbf{e} = \mathbf{0}, \tag{3.5}$$

$$\sum_{e \in E_0} \langle \mathbf{x}, \mathbf{e} \rangle \mathbf{e} = c\mathbf{x} \quad \text{for all } \mathbf{x} \in \mathbb{R}^d \text{ and for some } c > 0. \tag{3.6}$$



*Proof.* First, we define  $T: \mathbb{R}^d \rightarrow \mathbb{R}^d$  by  $T\mathbf{x} = \sum_{\mathbf{e} \in E_0} \langle \mathbf{x}, \mathbf{e} \rangle \mathbf{e}$ . Since

$$\langle T\mathbf{x}, \mathbf{y} \rangle = \sum_{\mathbf{e} \in E_0} \langle \mathbf{x}, \mathbf{e} \rangle \langle \mathbf{y}, \mathbf{e} \rangle = \langle \mathbf{x}, T\mathbf{y} \rangle, \quad (3.7)$$

we obtain that  $T$  is symmetric. We would prove that  $\Phi$  is a standard realization if and only if there exists a positive constant  $c > 0$  such that  $T = cI$ .

On the other hand, for any symmetric matrix  $T$  of size  $d$  with positive eigenvalues, there exists an orthogonal matrix  $P$  such that  $P^T T P = \text{diag}(\lambda_1, \dots, \lambda_d)$ , where  $\lambda_j > 0$  are eigenvalues of  $T$ . The inequality of arithmetic and geometric means implies

$$\text{tr } T = \text{tr } P^T T P \geq d(\det P^T T P)^{1/d} = d(\det T)^{1/d},$$

and the equality holds if and only if  $T = \lambda I_d$ .

Here, we write  $E_0 = \{e_\alpha\}_{\alpha=1}^{|E_0|}$ , and  $\mathbf{e}_i = (e_{\alpha 1}, \dots, e_{\alpha d}) \in \mathbb{R}^d$ . Since the equation (3.6) is equivalent to

$$\langle T\mathbf{x}, \mathbf{y} \rangle = \sum_{\mathbf{e} \in E_0} \langle \mathbf{e}, \mathbf{x} \rangle \langle \mathbf{e}, \mathbf{y} \rangle = c \langle \mathbf{x}, \mathbf{y} \rangle, \quad (3.8)$$

taking an orthogonal basis  $\{\mathbf{x}_j\}_{j=1}^d$  of  $\mathbb{R}^d$ , and set  $\mathbf{x} = \mathbf{x}_j$ , and  $\mathbf{y} = \mathbf{x}_k$ , we obtain

$$\sum_{\alpha=1}^{|E_0|} e_{\alpha j} e_{\alpha k} = c \delta_{jk}, \quad (3.9)$$

and

$$\text{Vol}(\Gamma)^{2/d} E(\Phi, \rho) = \sum_{\mathbf{e} \in E_0} |\mathbf{e}|^2 = \sum_{\alpha=1}^{|E_0|} \sum_{j=1}^d e_{\alpha j}^2 = cd. \quad (3.10)$$

Now, we assume that  $(\Phi_1, \rho_1)$  is a standard realization of  $X$  and  $(\Phi_2, \rho_2)$  is a harmonic realization of  $X$ . By Proposition 3.16, there exists an  $A = (a_{ij}) \in GL(d, \mathbb{R})$  and  $\mathbf{b} \in \mathbb{R}^d$  such that  $\Phi_2 = A\Phi_1 + \mathbf{b}$  and  $\rho_1 = A\rho_2$ . Then, we obtain

$$\text{Vol}(\Gamma_1) = |\det A| \text{Vol}(\Gamma_2), \quad f_{\alpha i} = \sum_{j=1}^d a_{ij} e_{\alpha j},$$

and

$$\begin{aligned} \text{Vol}(\Gamma_2)^{2/d} E(\Phi_2, \rho_2) &= \sum_{i=1}^d \sum_{\alpha=1}^{|E_0|} f_{\alpha i}^2 = \sum_{i=1}^d \sum_{j,k=1}^d \sum_{\alpha=1}^{|E_0|} a_{ij} a_{ik} e_{\alpha j} e_{\alpha k} \\ &= \sum_{i=1}^d \sum_{j,k=1}^d \sum_{\alpha=1}^{|E_0|} a_{ij} a_{ik} \delta_{jk} = c \sum_{i=1}^d \sum_{j=1}^d a_{ij} a_{ij} = c \text{tr } A^T A \\ &\geq cd(\det A^T A)^{1/d} = cd(\det A)^{2/d} = cd(\text{Vol}(\Gamma_2)/\text{Vol}(\Gamma_1))^{2/d} \\ &= cd \text{Vol}(\Gamma_2) E(\Phi_1, \rho_1). \end{aligned}$$

This implies that  $E(\Phi_2, \rho_2) \geq E(\Phi_1, \rho_1)$  if and only if the equation (3.6) holds.  $\square$

**Theorem 3.20** (Sunada [37, 38, 39]). *Assume that  $\Phi$  is a standard realization of a  $d$ -dimensional topological crystal. Then, each element  $\sigma \in \text{Aut}(X)$  extends as an element of  $\text{Aut}(\Phi(X)) \subset O(d) \times \mathbb{R}^d$  (Euclidean motion group of  $\mathbb{R}^d$ ).*

Theorem 3.20 means that standard realizations, which are obtained by a variational principle, have maximum symmetry among all the realizations of a topological crystal.

Recently, Kajigaya–Tanaka [14] study the existence of discrete harmonic maps into Riemann surface of genus greater than one.

**Example 3.21.** The realization (b) of Fig. 3.2 is a standard realization of a hexagonal lattices, whereas, the realization (c) of Fig. 3.2 is not a standard.

**Example 3.22.** Let  $\triangle ABC$  be a triangle on a plane and  $O$  be the barycenter of the triangle, and consider a graph  $G = (V, E)$  consisting  $V = \{O, A, B, C\}$  and  $E = \{(O, A), (O, B), (O, C)\}$ . By a property of the barycenter of triangles, we obtain  $\overrightarrow{OA} + \overrightarrow{OB} + \overrightarrow{OC} = \mathbf{0}$ . That is to say, the balancing condition (3.3) holds for  $O \in V$ ; however, the condition (3.6) only holds for the case that  $\triangle ABC$  is a regular triangle.

**Definition 3.23** (Sunada [37, 38, 39]). A topological crystal  $X$  of degree  $n$  is called *strongly isotropic*, if there exists  $g \in \text{Aut}(X)$  such that  $g(u) = v$  and  $g(e_i) = f_{\sigma(i)}$ , for any  $u, v \in V$ , and for any permutation  $\sigma \in \mathfrak{S}_n$ , where  $E_u = \{e_i\}_{i=1}^n$  and  $E_v = \{f_j\}_{j=1}^n$ .

**Theorem 3.24** (Sunada [37]). *2-dimensional strongly isotropic topological crystals are hexagonal lattices only. 3-dimensional strongly isotropic topological crystals are diamond lattices and  $K_4$  lattices (and their mirror image) only.*

**Remark 3.25.** A square lattice does not have the strongly isotropic property. Let  $X$  be a square lattice. Consider a vertex  $v \in V$ ,  $g = \text{id} \in \text{Aut}(X)$ , and let  $e_1, e_2, e_3, e_4 \in E_v$  be edges to north, west, south, and east. If  $X$  has the strongly isotropic property, then any  $\sigma \in \mathfrak{S}_4$ ,  $g(e_i) = e_{\sigma(i)}$  for  $i = 1, 2, 3, 4$ . However, we exchange edges by the permutation  $\sigma(1, 2, 3, 4) = (2, 1, 3, 4)$ , then, the graph structure could not preserved. Hence, a square lattice is not strongly isotropic.

Graphenes and diamonds have nice physical properties (see Section 3.3), and they are carbon structure of standard realizations of hexagonal and diamond lattices, which are strongly isotropic. Hence, we may expect that  $K_4$ -carbons are also nice physical properties.

**Remark 3.26.** Kotani–Sunada considered topological crystals from probabilistic motivations [18, 19, 22, 37]. A *random walk* on a graph  $X = (V, E)$  is a stochastic process associated with  $p: E \rightarrow [0, 1]$  satisfying  $\sum_{e \in E_x} p(e) = 1$ . In the case of  $p(e) = 1/|E_x|$ , the random walk is called *simple random walk*. The function  $p$  is considered as *transition probability* from  $o(e)$  to  $t(e)$ . Define  $p_X(n, x, y) = \sum p(e_1) \cdots p(e_n)$ , where summation over all paths with  $e = e_1 \cdots e_n$ ,  $o(e_1) = x$ ,  $t(e_n) = y \in V$ , is called  *$n$ -step probability* from  $x$  to  $y$ .

Let  $X$  be a  $d$ -dimensional topological crystal, Kotani–Sunada studied when the simple random walk on  $X$  “converges” to a Brownian motion on  $\mathbb{R}^d$  as the mesh of  $X$  becomes finer, and proved that if a realization of  $X$  is standard, then there exists constants  $C$  depending only on  $X$  such that

$$\frac{1}{\deg(y)} p_X(n, x, y) \sim \frac{C}{(4\pi n)^{d/2}} (1 + c_1(x, y)n^{-1} + O(n^{-2})) \text{ as } n \rightarrow \infty,$$

$$c_1(x, y) = -\frac{C}{4} |\mathbf{x} - \mathbf{y}|^2 + g(x) + g(y) + c, \text{ for certain } g \text{ and } c,$$

which means that  $p_X(n, x, y)$  “converges” to the heat kernel  $p_{\mathbb{R}^d}(t, \mathbf{x}, \mathbf{y})$  as  $n \uparrow \infty$ .

### 3.2 Explicit constructions of standard realizations

In this section, we demonstrate how to construct a standard realization from given base graph explicitly.

Let  $X_0 = (V_0, E_0)$  be a finite graph with  $d = \text{rank } H_1(X_0, \mathbb{Z})$ . We define a natural inner product on  $d$ -dimensional vector space  $C_1(X_0, \mathbb{R})$  by

$$\langle e_1, e_2 \rangle = \begin{cases} 1 & \text{if } e_1 = e_2, \\ -1 & \text{if } e_1 = \bar{e}_2, \\ 0 & \text{otherwise,} \end{cases}$$

for  $e_1, e_2 \in E_0$ . By using the inner product, we may identify  $C_1(X_0, \mathbb{R})$  to  $\mathbb{R}^{|E_0|}$ , hence we may also identify  $H_1(X_0, \mathbb{R})$  to  $\mathbb{R}^d$ .

Let  $X = (V, E)$  be the maximum abelian covering of  $X_0$ , and  $\pi: X \rightarrow X_0$  be the covering map. Fix a vertex  $v_0 \in V_0$ , and define  $\Phi: X \rightarrow H_1(X_0, \mathbb{R})$  by

$$\Phi(v) = P(\pi(e_1)) + \cdots + P(\pi(e_n)), \quad (3.11)$$

where  $e = e_1 \cdots e_n$  is a path in  $X$  connecting  $v_0 = o(e_1)$  and  $v = t(e_n)$ , and  $P: C_1(X_0, \mathbb{R}) \rightarrow H_1(X_0, \mathbb{R})$  is the orthogonal projection.

**Proposition 3.27** (Sunada [39]). *The map  $\Phi: X \rightarrow H_1(X_0, \mathbb{R})$  defined by (3.11) is a harmonic realization of  $X$ , namely,*

$$\sum_{e \in (E_0)_v} P(e) = 0 \in H_1(X_0, \mathbb{R}). \quad (3.12)$$

*Proof.* First, we prove that

$$\sum_{e \in (E_0)_v} \langle e, c \rangle = 0 \quad (3.13)$$

for an arbitrary closed path  $c = e_1 \cdots e_n$  in  $X_0$ . If  $c$  does not contain an edge whose origin or terminus is  $v$ , then the equation (3.13) obviously holds. Let  $e_j$  and  $e_{j+1}$  be edges in  $c$  satisfying  $t(e_j) = o(e_{j+1}) = v$ , then  $\langle e, e_j + e_{j+1} \rangle = 1 - 1 = 0$ . Hence, we obtain (3.13).

The equality (3.13) implies that

$$\sum_{e \in (E_0)_v} e \in H_1(X_0, \mathbb{R})^\perp,$$

since  $H_1(X_0, \mathbb{R})$  is generated by closed paths in  $X_0$ . Therefore, we obtain

$$0 = P \left( \sum_{e \in (E_0)_v} e \right) = \sum_{e \in (E_0)_v} P(e),$$

and hence we get (3.12).  $\square$

**Proposition 3.28** (Sunada [39]). *The map  $\Phi: X \rightarrow H_1(X_0, \mathbb{R})$  defined by (3.11) is a standard realization of  $X$ , namely, there exists a constant  $c > 0$  such that*

$$\sum_{e \in E_0} (\langle P(e), x \rangle)^2 = c|x|^2, \quad x \in H_1(X_0, \mathbb{R}). \quad (3.14)$$

*Proof.* Since the set of oriented edges  $E_0^o := \{e_i\}_{i=1}^n$  is an orthonormal basis of  $C_1(X_0, \mathbb{R})$ , we obtain

$$\sum_{e \in E_0^o} (\langle P(e), x \rangle)^2 = \sum_{e \in E_0^o} (\langle e, x \rangle)^2 = |x|^2,$$

and

$$\sum_{e \in E_0} (\langle P(e), x \rangle)^2 = \sum_{e \in E_0^o} (\langle P(e), x \rangle)^2 + \sum_{\bar{e} \in E_0^o} (\langle P(e), x \rangle)^2 = 2 \sum_{e \in E_0^o} (\langle P(e), x \rangle)^2,$$

hence we get (3.14)  $\square$

By the above arguments, the realization  $\Phi$  of  $X_0$  is into  $H_1(X_0, \mathbb{R})/H_1(X_0, \mathbb{Z})$  with the period lattice  $\Gamma$ . The torus  $H_1(X_0, \mathbb{R})/H_1(X_0, \mathbb{Z})$  is called an *Albanese torus*. Therefore, to calculate explicit coordinates of standard realizations, we should compute correspondences between the Albanese torus and  $\mathbb{R}^d/\mathbb{Z}^d$ .

### 3.2.1 Explicit algorithm in cases of maximum abelian coverings

Now we explain explicit algorithm to obtain a standard realization of a  $d$ -dimensional topological crystal  $X$ , which is a maximum abelian covering of  $X_0 = (V_0, E_0)$ . This method is followed by Sunada [39] and Naito [28]. In the followings, set  $b = \text{rank } H_1(X_0, \mathbb{Z})$ .

**Step 1** First, compute a spanning tree  $X_1 = (V_0, E_1)$  of  $X_0$  by Kruskal's algorithm, and set  $E_0 \setminus E_1 = \{e_i\}_{i=1}^b$  and  $E_1 = \{e_i\}_{i=b+1}^{|E|}$ . Then, we may select a  $\mathbb{Z}$ -basis  $\{\alpha_i\}_{i=1}^b$  of  $H_1(X_0, \mathbb{Z})$  as follows. For each edge  $e_i \in E_0 \setminus E_1$ , we may find a path  $p_i$  in  $E_1$  such that  $o(p_i) = t(e_i)$  and  $t(p_i) = o(e_i)$ . The path  $p_i e_i \in E_0$  is a closed path in  $E_0$ , and hence by Propositions 2.8 and 2.9, we may set  $\alpha_i = [p_i e_i]$ .

**Step 2** Since  $\{\alpha_i\}_{i=1}^b$  is a  $\mathbb{Z}$ -basis of  $H_1(X_0, \mathbb{Z})$ , for each edge  $e \in E_0$  there exists  $a_i(e) \in \mathbb{R}$  such that

$$P(e) = \sum_{i=1}^b a_i(e) \alpha_i \in H_1(X_0, \mathbb{R}). \quad (3.15)$$

Since  $e \in C_1(X_0, \mathbb{R})$  and  $P$  is the orthogonal projection from  $C_1(X_0, \mathbb{R})$  onto  $H_1(X_0, \mathbb{R})$ .  $P(e)$  satisfies

$$\langle P(e) - e, \alpha_j \rangle = 0, \text{ for any } j. \quad (3.16)$$

Substituting (3.15) into (3.16), we obtain

$$\sum_{i=1}^b a_i(e) \langle \alpha_i, \alpha_j \rangle = \langle e, \alpha_j \rangle. \quad (3.17)$$

Set  $A = (\langle \alpha_i, \alpha_j \rangle) \in GL(b, \mathbb{R})$ , and  $\mathbf{a}(e) = (a_i(e))^T$ ,  $\mathbf{b}(e) = (\langle e, \alpha_i \rangle)^T \in \mathbb{R}^b$ , then (3.17) is written as

$$\mathbf{a}(e) = A^{-1} \mathbf{b}(e). \quad (3.18)$$

We get  $\mathbf{a}(e)$  for each  $e \in E_0$ , then we obtain the realization

$$P(e) = \mathbf{e} = \sum_{i=1}^b a_i(e) \alpha_i, \text{ in } H_1(X_0, \mathbb{R}). \quad (3.19)$$

On the other hand, we easily calculate  $\mathbf{b}(e)$  and  $A$ , since  $e$  and  $\alpha_i$  are given by linear combinations of  $\{e_i\}_{i=1}^b$  and  $\{e_i\}_{i=b+1}^{|E|}$ . Therefore, by (3.18), we obtain  $\mathbf{a}(e)$ . We remark that the matrix  $A$  is the Gram matrix of the basis  $\{\alpha_i\}_{i=1}^b$ . Taking an orthonormal basis  $\{\mathbf{x}_i\}_{i=1}^b$  of  $H_1(X_0, \mathbb{R})$  and write

$$\alpha_i = \sum_{j=1}^b \beta_{ij} \mathbf{x}_j, \quad (3.20)$$

then we obtain the expression of the realization in the Cartesian coordinates of  $H_1(X_0, \mathbb{R}) \cong \mathbb{R}^b$  as

$$\mathbf{e} = \sum_{i=1}^b a_i(e) \alpha_i = \sum_{i=1}^b \left( \sum_{j=1}^b a_i(e) \beta_{ij} \right) \mathbf{x}_j \text{ for } e \in E_0. \quad (3.21)$$

To obtain the relation (3.20), we may use the Cholesky decomposition. The Cholesky decomposition, which is a special case of  $LU$  decomposition, gives us the decomposition  $A = X^T X$  for any positive definite symmetric matrix  $A$  by an upper triangular matrix  $X$  (see for example [35]).

**Step 3** Fix a vertex  $v_0 \in V_0$ , and set  $\mathbf{v}_0 = \mathbf{0}$  (origin of  $\mathbb{R}^b$ ). For each vertex  $v_j \in V_0$ , we find the shortest path  $e = e_{j1} \cdots e_{jk} \in E_1$  with  $o(e_{j1}) = v_0$  and  $t(e_{jk}) = v_j$ , which is a shortest path in the spanning tree finding in Step 1 connecting  $v_0$  and  $v_j$ . By using (3.19), we obtain

$$\mathbf{v}_j = \sum_{i=1}^k \mathbf{e}_{ji} = \sum_{i=1}^k \sum_{k=1}^b a_k(e_{ji}) \alpha_k. \quad (3.22)$$

In the above, we realize edges in the spanning tree. Hence, to complete calculation, we compute realizations of edges which are not contained in the spanning tree. For each  $e_\ell \in E_0 \setminus E_1$ , we define  $\mathbf{w}_\ell \in \mathbb{R}^b$  by

$$\mathbf{w}_\ell = \mathbf{v}(e_\ell) + \mathbf{e}_\ell, \quad (3.23)$$

where  $\mathbf{v}(e_\ell) = o(e_\ell)$ .

Vertices  $\{\mathbf{v}_j\}_{j=1}^{|V|} \sqcup \{\mathbf{w}_\ell\}_{\ell=1}^b \subset \mathbb{R}^b$  (or edges  $\{\mathbf{e}_i\}_{i=1}^{|E_0|}$ ) with the period lattice  $\{\alpha_i\}_{i=1}^b$  give us a standard realization of  $X$  with period lattice  $\Gamma$ . The set of realizations of edges  $\{\mathbf{e}_j\}_{j=1}^{|E|}$  is called the *building block*. In other words, Information of adjacency of the graph and the building block give us a standard realization.

**Remark 3.29.** Dijkstra's algorithm gives us shortest paths from a vertex to any other vertices within  $O(|E| + |V| \log |V|)$  (see for example [1]).

**Example 3.30 (Square lattices in  $\mathbb{R}^2$ , Fig. 3.1 (a), Sunada [39, Section 8.3]).** The base graph  $X_0 = (V_0, E_0)$  of square lattices in  $\mathbb{R}^2$  is the 2-bouquet graph (Fig. 3.3 (a)), and  $\text{rank } H_1(X_0, \mathbb{R}) = 2$ . Write  $V_0 = \{v_0\}$  and  $E_0 = \{e_1, e_2\}$ , as in Fig. 3.3 (a), then a spanning tree of  $X_0$  is  $X_1 = (V_0, \{\emptyset\})$ , namely,  $E_1 = \{\emptyset\}$ . Hence, we may take  $\alpha_1 = e_1$  and  $\alpha_2 = e_2$  as a  $\mathbb{Z}$ -basis of  $H_1(X_0, \mathbb{Z})$ , and obtain

$$\begin{aligned} A &= \begin{bmatrix} \langle \alpha_1, \alpha_1 \rangle & \langle \alpha_1, \alpha_2 \rangle \\ \langle \alpha_2, \alpha_1 \rangle & \langle \alpha_2, \alpha_2 \rangle \end{bmatrix} = \begin{bmatrix} 1 & 0 \\ 0 & 1 \end{bmatrix}, \quad A^{-1} = A, \\ [\mathbf{b}(e_1) \quad \mathbf{b}(e_2)] &= \begin{bmatrix} \langle e_1, \alpha_1 \rangle & \langle e_2, \alpha_1 \rangle \\ \langle e_1, \alpha_2 \rangle & \langle e_2, \alpha_2 \rangle \end{bmatrix} = \begin{bmatrix} 1 & 0 \\ 0 & 1 \end{bmatrix}, \\ [\mathbf{a}(e_1) \quad \mathbf{a}(e_2)] &= A [\mathbf{b}(e_1) \quad \mathbf{b}(e_2)] = \begin{bmatrix} 1 & 0 \\ 0 & 1 \end{bmatrix}. \end{aligned}$$

On the other hand, the shortest paths from  $\mathbf{v}_0$  to other vertices are

$$\text{spath}(\mathbf{v}_0, \mathbf{w}_i) = (\mathbf{v}_0 \mathbf{w}_i), \quad i = 1, 2.$$

Since  $\{\alpha_i\}_{i=1}^2$  is orthonormal, hence, we obtain

$$\mathbf{v}_0 = \begin{bmatrix} 0 \\ 0 \end{bmatrix}, \quad \mathbf{w}_1 = \mathbf{v}_0 + a(e_1) = \begin{bmatrix} 1 \\ 0 \end{bmatrix}, \quad \mathbf{w}_2 = \mathbf{v}_0 + a(e_2) = \begin{bmatrix} 0 \\ 1 \end{bmatrix},$$

and the period lattice is

$$[\mathbf{x}_1 \quad \mathbf{x}_2] = \begin{bmatrix} 1 & 0 \\ 0 & 1 \end{bmatrix}.$$

The above datas allows us to write figure in Fig. 3.1 (a).

**Example 3.31 (Hyper-cubic lattice in  $\mathbb{R}^n$ , Sunada [39, Section 8.3]).** A generalization of Example 3.30 is hyper-cubic lattices in  $\mathbb{R}^n$ . In case of  $n = 3$ , it is called cubic lattices. The base graph  $X_0 = (V_0, E_0)$  of hyper-cubic lattices is the  $n$ -bouquet graph (Fig. 3.3 (b)), namely  $V_0 = \{v\}$ ,  $E_0 = \{e_i\}_{i=1}^n$ , as in Fig. 3.3 (b). Since a spanning tree of  $X_0$  is  $X_1 = (V_0, \{\emptyset\})$ , we may take an orthonormal  $\mathbb{Z}$ -basis of  $H_1(X_0, \mathbb{Z})$  by  $\{\alpha_i\}_{i=1}^n$ , where  $\alpha_i = e_i$ . By similar calculations, we obtain

$$A = A^{-1} = [a(e_i)] = [b(e_i)] = E_n \quad (\text{the identity matrix of size } n).$$

Hence, we obtain

$$\mathbf{v}_0 = \mathbf{0}, \quad \mathbf{w}_i = \mathbf{x}_i \quad (\text{standard } i\text{-th unit vector of } \mathbb{R}^n) \quad i = 1, \dots, n,$$

and the period lattice is  $[\mathbf{x}_i] = E_n$ . A standard realization of hyper-cubic lattices is an orthonormal lattice in  $\mathbb{R}^n$ .

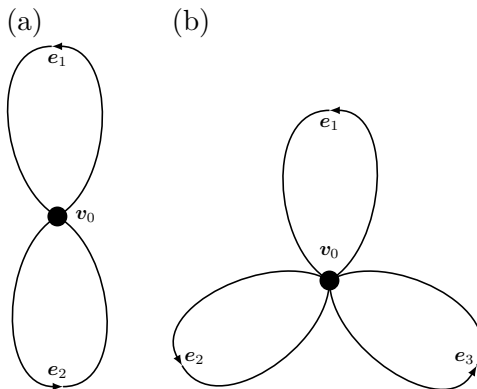


Figure 3.3: (a) The 2-bouquet graph, which is the base graph of square lattices, (b) the 3-bouquet graph, which is the base graph of cubic lattices.

**Example 3.32 (Hexagonal lattices, Fig. 3.1 (c), Sunada [39, Section 8.3]).** The base graph  $X_0 = (V_0, E_0)$  of hexagonal lattices in  $\mathbb{R}^2$  is the graph with two vertices and three edges connecting both vertices (Fig. 3.4 (a)), and  $\text{rank } H_1(X_0, \mathbb{R}) = 2$ . Write  $V_0 = \{v_0, v_1\}$  and  $E_0 = \{e_1, e_2, e_3\}$  as in Fig. 3.4, then a spanning tree of  $X_0$  is  $X_1 = (V_0, \{e_3\})$ . Hence, we may take  $\alpha_1 = e_1 - e_3$  and  $\alpha_2 = e_2 - e_3$  as a  $\mathbb{Z}$ -basis of  $H_1(X_0, \mathbb{Z})$ , and obtain

$$A = \begin{bmatrix} 2 & 1 \\ 1 & 2 \end{bmatrix}, \quad A^{-1} = \frac{1}{3} \begin{bmatrix} 2 & -1 \\ -1 & 2 \end{bmatrix}$$

$$[\mathbf{b}(e_1) \quad \mathbf{b}(e_2) \quad \mathbf{b}(e_3)] = \begin{bmatrix} 1 & 0 & -1 \\ 0 & 1 & -1 \end{bmatrix},$$

$$[\mathbf{a}(e_1) \quad \mathbf{a}(e_2) \quad \mathbf{a}(e_3)] = \frac{1}{3} \begin{bmatrix} 2 & -1 & -1 \\ -1 & 2 & -1 \end{bmatrix}.$$

The shortest paths from  $\mathbf{v}_0$  to other vertices are

$$\text{spath}(\mathbf{v}_0, \mathbf{w}_i) = (\mathbf{v}_0 \mathbf{w}_i) \quad i = 1, 2.$$

Since  $\{\alpha_i\}_{i=1}^2$  is not orthonormal, we choice the basis as

$$\begin{bmatrix} \alpha_1 \\ \alpha_2 \end{bmatrix} = \begin{bmatrix} \sqrt{2} & 0 \\ 1/\sqrt{2} & \sqrt{3/2} \end{bmatrix} =: X,$$

then we obtain

$$\begin{aligned} \mathbf{v}_0 &= \mathbf{0}, \\ \mathbf{w}_1 &= \frac{2}{3}\alpha_1 - \frac{1}{3}\alpha_2 = \begin{bmatrix} 1/\sqrt{2} \\ -1/\sqrt{6} \end{bmatrix}, \\ \mathbf{w}_2 &= -\frac{1}{3}\alpha_1 + \frac{2}{3}\alpha_2 = \begin{bmatrix} 0 \\ \sqrt{2/3} \end{bmatrix}, \\ \mathbf{w}_3 &= -\frac{1}{3}\alpha_1 - \frac{1}{3}\alpha_2 = \begin{bmatrix} -1/\sqrt{2} \\ -1/\sqrt{6} \end{bmatrix}, \end{aligned}$$

and the period lattice is

$$[\mathbf{x}_1 \quad \mathbf{x}_2] = X.$$

Note that  $\langle \mathbf{w}_i, \mathbf{w}_j \rangle = (-1/2)|\mathbf{w}_i||\mathbf{w}_j|$  ( $i \neq j$ ) are satisfied. The above datas allow us to write figure in Fig. 3.1 (c).

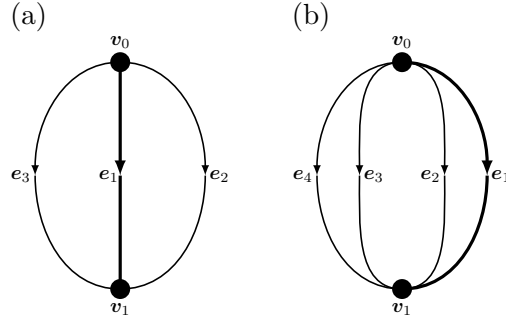


Figure 3.4: (a) The base graph of hexagonal lattices, (b) the base graph of diamond lattices. Thick edges consist a spanning tree of them.

**Example 3.33 (Diamond lattices, Sunada [39, Section 8.3]).** The base graph  $X_0 = (V_0, E_0)$  of a diamond lattices in  $\mathbb{R}^3$  is the graph with two vertices and four edges connecting both vertices, and  $\text{rank } H_1(X_0, \mathbb{R}) = 3$  (see Fig. 3.18). Write  $V_0 = \{v_0, v_1\}$  and  $E_0 = \{e_1, e_2, e_3, e_4\}$ , where  $e_i = (v_0, v_1)$ , then a spanning tree of  $X_0$  is  $X_1 = (V_0, \{e_4\})$ . Hence, we may take  $\alpha_i = e_i - e_4$  ( $i = 1, 2, 3$ ) as a  $\mathbb{Z}$ -basis of  $H_1(X_0, \mathbb{Z})$ , and obtain

$$\begin{aligned} A &= \begin{bmatrix} 2 & 1 & 1 \\ 1 & 2 & 1 \\ 1 & 1 & 2 \end{bmatrix}, \quad A^{-1} = \frac{1}{4} \begin{bmatrix} 3 & -1 & -1 \\ -1 & 3 & -1 \\ -1 & -1 & 3 \end{bmatrix} \\ [\mathbf{b}(e_1) \quad \mathbf{b}(e_2) \quad \mathbf{b}(e_3) \quad \mathbf{b}(e_4)] &= \begin{bmatrix} 1 & 0 & 0 & -1 \\ 0 & 1 & 0 & -1 \\ 0 & 0 & 1 & -1 \end{bmatrix}, \\ [\mathbf{a}(e_1) \quad \mathbf{a}(e_2) \quad \mathbf{a}(e_3) \quad \mathbf{a}(e_4)] &= \frac{1}{4} \begin{bmatrix} 3 & -1 & -1 & -1 \\ -1 & 3 & -1 & -1 \\ -1 & -1 & 3 & -1 \end{bmatrix}, \\ \begin{bmatrix} \alpha_1 \\ \alpha_2 \\ \alpha_3 \end{bmatrix} &= \begin{bmatrix} \sqrt{2} & 0 & 0 \\ 1/\sqrt{2} & \sqrt{3/2} & 0 \\ 1/\sqrt{2} & 1/\sqrt{6} & 2/\sqrt{3} \end{bmatrix} =: X. \end{aligned}$$

The shortest paths from  $\mathbf{v}_0$  to other vertices are

$$\text{spath}(\mathbf{v}_0, \mathbf{w}_i) = (\mathbf{v}_0 \mathbf{w}_i) \quad i = 1, 2, 3.$$

Hence, we obtain

$$\begin{aligned}
\mathbf{v}_0 &= \mathbf{0}, \\
\mathbf{w}_1 &= \frac{3}{4}\alpha_1 - \frac{1}{4}\alpha_2 - \frac{1}{4}\alpha_3 = \begin{bmatrix} 1/\sqrt{2} \\ -1/\sqrt{6} \\ -1/(2\sqrt{3}) \end{bmatrix}, \\
\mathbf{w}_2 &= -\frac{1}{4}\alpha_1 + \frac{3}{4}\alpha_2 - \frac{1}{4}\alpha_3 = \begin{bmatrix} 0 \\ \sqrt{2/3} \\ -1/(2\sqrt{3}) \end{bmatrix}, \\
\mathbf{w}_3 &= -\frac{1}{4}\alpha_1 - \frac{1}{4}\alpha_2 + \frac{3}{4}\alpha_3 = \begin{bmatrix} 0 \\ 0 \\ 2/\sqrt{3} \end{bmatrix}, \\
\mathbf{w}_4 &= -\frac{1}{4}\alpha_1 - \frac{1}{4}\alpha_2 - \frac{1}{4}\alpha_3 = \begin{bmatrix} -1/\sqrt{2} \\ -1/\sqrt{6} \\ -1/(2\sqrt{3}) \end{bmatrix}.
\end{aligned}$$

The period lattice is

$$[\mathbf{x}_1 \quad \mathbf{x}_2 \quad \mathbf{x}_3] = X.$$

Note that  $\langle \mathbf{w}_i, \mathbf{w}_j \rangle = (-1/3)|\mathbf{w}_i||\mathbf{w}_j|$  ( $i \neq j$ ) are satisfied.

**Example 3.34 (Gyroid lattices ( $K_4$  lattices), Sunada [39, Section 8.3]).** The base graph  $X_0 = (V_0, E_0)$  of a gyroid lattices in  $\mathbb{R}^3$  is the  $K_4$  graph, which is the complete graph of four vertices, and  $\text{rank } H_1(X_0, \mathbb{R}) = 3$ . Write  $V_0 = \{v_i\}_{i=1}^4$  and  $E_0 = \{e_i\}_{i=1}^6$  as in Fig. 3.5 (a), and take a spanning tree  $X_1$  of  $X_0$  as in Fig. 3.5 (b). Hence, we may take

$$\alpha_1 = e_1 + e_4 - e_2, \quad \alpha_2 = e_2 + e_5 - e_3, \quad \alpha_3 = e_3 + e_6 - e_1$$

as a  $\mathbb{Z}$ -basis of  $H_1(X_0, \mathbb{Z})$ , and obtain

$$\begin{aligned}
A &= \begin{bmatrix} 3 & -1 & -1 \\ -1 & 3 & -1 \\ -1 & -1 & 3 \end{bmatrix}, \quad A^{-1} = \frac{1}{4} \begin{bmatrix} 2 & 1 & 1 \\ 1 & 2 & 1 \\ 1 & 1 & 2 \end{bmatrix} \\
\mathbf{b} &= \begin{bmatrix} 1 & -1 & 0 & 1 & 0 & 0 \\ 0 & 1 & -1 & 0 & 1 & 0 \\ -1 & 0 & 1 & 0 & 0 & 1 \end{bmatrix}, \quad \mathbf{a} = \frac{1}{4} \begin{bmatrix} 1 & -1 & 0 & 2 & 1 & 1 \\ 0 & 1 & -1 & 1 & 2 & 1 \\ -1 & 0 & 1 & 1 & 1 & 2 \end{bmatrix}, \\
\begin{bmatrix} \alpha_1 \\ \alpha_2 \\ \alpha_3 \end{bmatrix} &= \begin{bmatrix} \sqrt{3} & 0 & 0 \\ -1/\sqrt{3} & 2\sqrt{2/3} & 0 \\ -1/\sqrt{3} & -\sqrt{2/3} & \sqrt{2} \end{bmatrix} =: X,
\end{aligned}$$

Let  $\{w_i\}_{i=1}^3$  be as in Fig. 3.5 (b), then the shortest paths from  $\mathbf{v}_0$  to other vertices are

$$\text{spath}(\mathbf{v}_0, \mathbf{v}_i) = (\mathbf{v}_0 \mathbf{v}_i), \quad \text{spath}(\mathbf{v}_0, \mathbf{w}_i) = (\mathbf{v}_0 \mathbf{v}_i)(\mathbf{v}_i \mathbf{w}_i), \quad i = 1, 2, 3.$$



Hence, we obtain

$$\begin{aligned}
\mathbf{v}_0 &= \mathbf{0}, \\
\mathbf{v}_1 &= \frac{1}{4}\alpha_1 - \frac{1}{4}\alpha_3 = \begin{bmatrix} 1/\sqrt{3} \\ 1/(2\sqrt{6}) \\ -1/(2\sqrt{2}) \end{bmatrix}, & \mathbf{w}_1 &= \mathbf{v}_1 + \frac{1}{2}\alpha_1 + \frac{1}{4}\alpha_2 + \frac{1}{4}\alpha_3 = \begin{bmatrix} 2/\sqrt{3} \\ 1/\sqrt{6} \\ 0 \end{bmatrix} \\
\mathbf{v}_2 &= \frac{1}{4}\alpha_2 - \frac{1}{4}\alpha_1 = \begin{bmatrix} -1/\sqrt{3} \\ 1/\sqrt{6} \\ 0 \end{bmatrix}, & \mathbf{w}_2 &= \mathbf{v}_2 + \frac{1}{4}\alpha_1 + \frac{1}{2}\alpha_2 + \frac{1}{4}\alpha_3 = \begin{bmatrix} -1/\sqrt{3} \\ 5/(2\sqrt{6}) \\ 1/(2\sqrt{2}) \end{bmatrix} \\
\mathbf{v}_3 &= \frac{1}{4}\alpha_3 - \frac{1}{4}\alpha_2 = \begin{bmatrix} 0 \\ -(1/2)\sqrt{3/2} \\ 1/(2\sqrt{2}) \end{bmatrix}, & \mathbf{w}_3 &= \mathbf{v}_3 + \frac{1}{4}\alpha_1 + \frac{1}{4}\alpha_2 + \frac{1}{2}\alpha_3 = \begin{bmatrix} 0 \\ -(1/2)\sqrt{3/2} \\ 3/(2\sqrt{2}) \end{bmatrix}.
\end{aligned}$$

A gyroid lattice is called a  $K_4$  lattice since its base graph is  $K_4$ . It is also called a Laves' graph of girth ten, a  $(10,3)$ - $a$  network, and a diamond twin. The minimum length of closed path (without backtracking paths) is called the *girth* of the graph. The girth of a gyroid lattice is 10 (see Fig. 3.8), and hence, it is called  $(10,3)$ - $a$  network.

**Remark 3.35.** We can also take coordinates which all vertices have rational numbers. Taking

$$\begin{bmatrix} \alpha_1 \\ \alpha_2 \\ \alpha_3 \end{bmatrix} = \begin{bmatrix} -1 & 1 & -1 \\ -1 & -1 & 1 \\ 1 & -1 & -1 \end{bmatrix},$$

then

$$\mathbf{v}_1 = \frac{1}{2} \begin{bmatrix} 0 \\ -1 \\ 1 \end{bmatrix}, \quad \mathbf{v}_2 = \frac{1}{2} \begin{bmatrix} 1 \\ 0 \\ -1 \end{bmatrix}, \quad \mathbf{v}_3 = \begin{bmatrix} -1 \\ 1 \\ 0 \end{bmatrix}, \quad \mathbf{w}_1 = \frac{1}{2} \begin{bmatrix} -1 \\ -2 \\ 1 \end{bmatrix}, \quad \mathbf{w}_2 = \begin{bmatrix} 1 \\ -1 \\ -2 \end{bmatrix}, \quad \mathbf{w}_3 = \begin{bmatrix} -2 \\ 1 \\ -1 \end{bmatrix}.$$

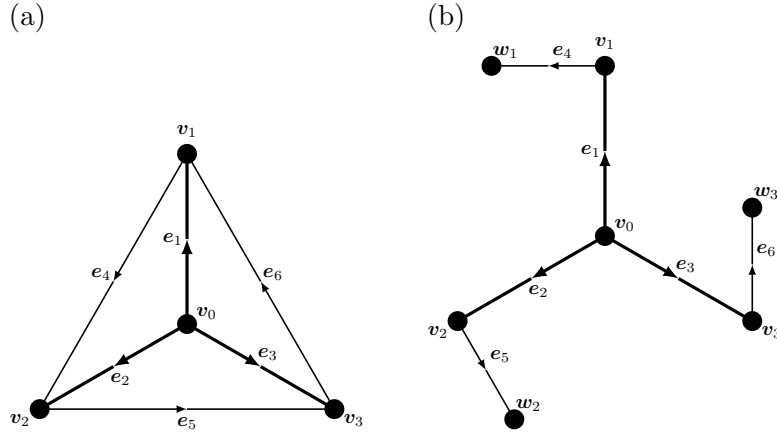


Figure 3.5: (a) The base graph of gyroid ( $K_4$ ) lattices, thick edges consist a spanning tree of them. (b) building block (in the abstract graph) of gyroid lattices.

**Remark 3.36.** Let  $\Phi(X)$  be a standard realization of diamond or cubic lattices, and  $C \in O(3) \setminus SO(3)$ . Then,  $C(\Phi(X))$  and  $\Phi(X)$  are mutually congruent, namely,  $\Phi(X)$  and its mirror image are mutually congruent in  $\mathbb{R}^3$ . This property is called *chiral symmetry*. On the other hand, a standard realization of  $K_4$  lattices is not chiral symmetric. Taking a  $C \in O(3) \setminus SO(3)$ ,  $X' = XC$  and constructing the realization as in Example 3.34, then we obtain a chiral image of  $\Phi(X)$ .

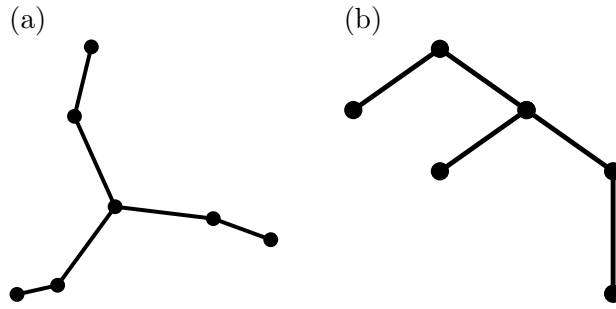


Figure 3.6: (a) A building block of a gyroid lattice ( $K_4$  lattice) viewed from a perpendicular direction of the plane consisted by  $\mathbf{v}_1$ ,  $\mathbf{v}_2$ , and  $\mathbf{v}_3$ , (b) one viewed from a parallel direction of it.

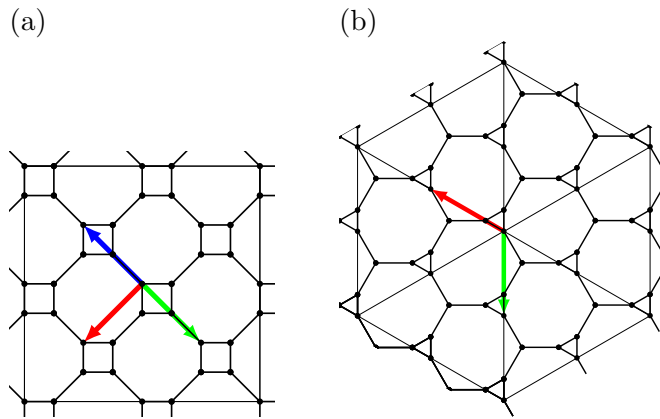


Figure 3.7: A gyroid ( $K_4$ ) lattice from (a)  $(0, 0, 1)$ -direction and (b)  $(1, 1, 1)$ -direction by using coordinates in Remark 3.35. The blue, red, and green vectors are  $\alpha_1$ ,  $\alpha_2$ , and  $\alpha_3$ , respectively. In (b),  $\alpha_1$  is the vector perpendicular to the paper from the back to the front.

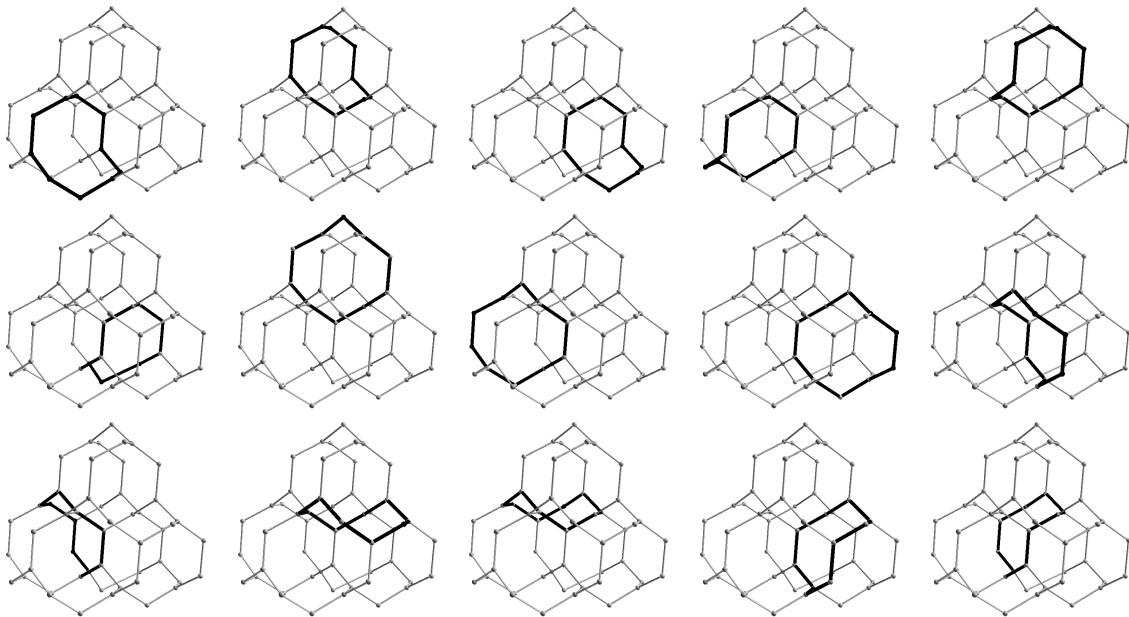


Figure 3.8: Fifteen 10-members rings pass through a vertex in a gyroid lattice. Each ring is mutually congruent.

### 3.2.2 Explicit algorithm for generic cases

In general, a standard realization of  $d$ -dimensional topological crystal  $X$  is not maximal abelian covering of a base graph  $X_0$ . In this section, we assume that  $d < b = \text{rank } H_1(X_0, \mathbb{Z})$ , and explain explicit algorithm to obtain a standard realization of  $X$ . This method is followed by Sunada [39].

Since  $d < b$ , the standard realization is constructed in a  $d$ -dimensional subspace  $V$  of  $H_1(X_0, \mathbb{R})$ , whose orthogonal subspace  $H$  is called the *vanishing subspace*, namely,  $H_1(X_0, \mathbb{R}) = V \oplus H$ , and  $V = H^\perp$  with  $\dim H = b - d$ .

**Step 1** By using the method of Step 1 in Section 3.2.1, find a  $\mathbb{Z}$ -basis  $\{\alpha_i\}_{i=1}^b$  of  $H_1(X_0, \mathbb{Z})$ , such that  $\{\alpha_i\}_{i=d+1}^b$  is a basis of the vanishing subspace  $H$ , using a linear transformation if necessary.

**Step 2** Compute  $A$ ,  $\mathbf{b}(e)$ , and  $\mathbf{a}(e)$  as in Step 2 of Section 3.2.1, then we obtain a standard realization of a topological crystal  $\tilde{X}$ , which is a maximal abelian covering of the base graph  $X_0$ . This realization  $\Phi^{\max}$  is in  $H_1(X_0, \mathbb{R}) \cong \mathbb{R}^b$ .

**Step 3** Let  $p: H_1(X_0, \mathbb{R}) \rightarrow H$  be the orthogonal projection, then  $\{\beta_i\}_{i=1}^d$  is a  $\mathbb{Z}$ -basis of the period lattice, where  $\beta_i = p(\alpha_i)$ . We should obtain  $B = (\langle \beta_i, \beta_j \rangle) \in GL(d, \mathbb{R})$  to calculate standard realizations of  $X$ . Since  $\gamma_i - \alpha_i = p(\alpha_i) - \alpha_i \in H$ , we may write

$$p(\alpha_i) = \alpha_i + \sum_{j=b+1}^d d_{ij} \alpha_j$$

and  $\langle p(\alpha_i), \alpha_k \rangle = 0$  for  $k = b + 1, \dots, d$ , and hence we obtain

$$\langle \alpha_i, \alpha_k \rangle = - \sum_{j=b+1}^d d_{ij} \langle \alpha_j, \alpha_k \rangle, \quad k = b + 1, \dots, d, \quad i = 1, \dots, b. \quad (3.24)$$

Write  $A = \begin{bmatrix} A_{11} & A_{12} \\ A_{21} & A_{22} \end{bmatrix}$ , where  $A_{11}$  is  $d \times d$  matrix,  $A_{22}$  is  $(b - d) \times (b - d)$  matrix,  $A_{12}^T = A_{21}$ , and  $D = (d_{ij})$ , then (3.24) implies

$$A_{12} = -DA_{22}. \quad (3.25)$$

Therefore, we obtain

$$\begin{aligned} \langle \beta_i, \beta_j \rangle &= \langle p(\alpha_i), p(\alpha_j) \rangle = \langle p^T p(\alpha_i), \alpha_j \rangle = \langle p(\alpha_i), \alpha_j \rangle \\ &= \left\langle \alpha_i + \sum_{k=b+1}^d d_{ik} \alpha_k, \alpha_j \right\rangle = \langle \alpha_i, \alpha_j \rangle + \sum_{k=b+1}^d d_{ik} \langle \alpha_k, \alpha_j \rangle, \end{aligned} \quad (3.26)$$

and thus, by (3.26), we obtain

$$B = A_{11} + DA_{21} = A_{11} - A_{12}A_{22}^{-1}A_{21}. \quad (3.27)$$

Since realizations of an edge  $e \in E_0$  of the maximal abelian covering of  $X_0$  is written as  $\mathbf{e}^{\max} = \sum_{i=1}^b a(e)\alpha_i$ , combining  $P: C_1(X_0, \mathbb{R}) \rightarrow H_1(X_0, \mathbb{R})$  and  $p: H_1(X_0, \mathbb{R}) \rightarrow H$ , we obtain

$$p(P(e)) = p(\mathbf{e}^{\max}) = \mathbf{e} = \sum_{i=1}^d a(e)\beta_i. \quad (3.28)$$

**Example 3.37 (Triangular lattice, Fig. 3.1 (b), Sunada [39, Section 8.3]).** A triangular lattice is the projection of a cubic lattice in  $\mathbb{R}^3$  onto a suitable 2-dimensional plane. Hence,  $d = 2$  and  $b = \text{rank } H_1(X_0, \mathbb{R}) = 3$ , and the base graph  $X_0 = (V_0, E_0)$  of triangular lattices is the one of cubic lattices, i. e.,  $X_0$  is the 3-bouquet graph (3.3). Using notation in Example 3.31, take  $\alpha_1 = e_1$ ,  $\alpha_2 = e_2$ ,  $\alpha_3 = e_1 + e_2 + e_3$ , and  $H = \text{span}\{\alpha_1, \alpha_2\}$ , then we obtain

$$A = \begin{bmatrix} 1 & 0 & 1 \\ 0 & 1 & 1 \\ 1 & 1 & 3 \end{bmatrix}, \quad \mathbf{b}(e) = \begin{bmatrix} 1 & 0 & 0 \\ 0 & 1 & 0 \\ 1 & 1 & 1 \end{bmatrix}, \quad \mathbf{a}(e) = \begin{bmatrix} 1 & 0 & -1 \\ 0 & 1 & -1 \\ 0 & 0 & 1 \end{bmatrix}, \quad (3.29)$$

and

$$\mathbf{e}_1^{\max} = \alpha_1, \quad \mathbf{e}_2^{\max} = \alpha_2, \quad \mathbf{e}_3^{\max} = -\alpha_1 - \alpha_2 + \alpha_3. \quad (3.30)$$

By (3.28) and (3.30), we obtain

$$\mathbf{e}_1 = \beta_1, \quad \mathbf{e}_2 = \beta_2, \quad \mathbf{e}_3 = -\beta_1 - \beta_2, \quad (3.31)$$

and by (3.27) and (3.29), we also obtain

$$B = [\langle \beta_i, \beta_j \rangle] = \begin{bmatrix} 1 & 0 \\ 0 & 1 \end{bmatrix} - \frac{1}{3} \begin{bmatrix} 1 \\ 1 \end{bmatrix} \begin{bmatrix} 1 & 1 \end{bmatrix} = \begin{bmatrix} 1 & 0 \\ 0 & 1 \end{bmatrix} - \frac{1}{3} \begin{bmatrix} 1 & 1 \\ 1 & 1 \end{bmatrix} = \frac{1}{3} \begin{bmatrix} 2 & -1 \\ -1 & 2 \end{bmatrix}.$$

On the other hand, the shortest paths from  $\mathbf{v}_0$  to other vertices are

$$\text{spath}(\mathbf{v}_0, \mathbf{v}_i) = (\mathbf{v}_0 \mathbf{v}_i) = \mathbf{e}_i \quad i = 1, 2, 3.$$

By using the Cholesky decomposition, we may write

$$\begin{bmatrix} \beta_1 \\ \beta_2 \end{bmatrix} = \begin{bmatrix} \sqrt{2/3} & -1/\sqrt{6} \\ 0 & 1/\sqrt{2} \end{bmatrix},$$

and hence by (3.31), we obtain

$$\mathbf{e}_1 = \begin{bmatrix} \sqrt{2/3} \\ 0 \end{bmatrix}, \quad \mathbf{e}_2 = \begin{bmatrix} -1/\sqrt{6} \\ 1/\sqrt{2} \end{bmatrix}, \quad \mathbf{e}_3 = \begin{bmatrix} -1/\sqrt{6} \\ -1/\sqrt{2} \end{bmatrix},$$

and

$$\mathbf{v}_0 = \begin{bmatrix} 0 \\ 0 \end{bmatrix}, \quad \mathbf{v}_1 = \mathbf{v}_0 + \mathbf{e}_1 = \begin{bmatrix} \sqrt{2/3} \\ 0 \end{bmatrix}, \quad \mathbf{v}_2 = \mathbf{v}_0 + \mathbf{e}_2 = \begin{bmatrix} -1/\sqrt{6} \\ 1/\sqrt{2} \end{bmatrix}, \quad \mathbf{v}_3 = \mathbf{v}_0 + \mathbf{e}_3 = \begin{bmatrix} -1/\sqrt{6} \\ -1/\sqrt{2} \end{bmatrix}.$$

The above datas allow us to write figure in Fig. 3.1 (b) (see also Fig. 3.9).

**Example 3.38 (Kagome lattice, Fig. 3.1 (d), Sunada [39, Section 8.3]).** A kagome lattice is a standard realization in  $\mathbb{R}^2$  whose base graph  $X_0$  shown in Fig. 3.11 (a). The graph  $X_0$  satisfies  $b = \text{rank } H_1(X_0, \mathbb{R}) = 4$ , and we may select

$$\alpha_1 = e_1 - e_4, \quad \alpha_2 = e_2 - e_5, \quad \alpha_3 = e_1 + e_2 + e_3, \quad \alpha_4 = e_4 + e_5 + e_6,$$

and  $H = \text{span}\{e_1 + e_2 + e_3, e_4 + e_5 + e_6\}$ . Then, we obtain

$$A = \begin{bmatrix} 2 & 0 & 1 & -1 \\ 0 & 2 & 1 & -1 \\ 1 & 1 & 3 & 0 \\ -1 & -1 & 0 & 3 \end{bmatrix}, \quad \mathbf{b}(e) = \begin{bmatrix} 1 & 0 & 0 & -1 & 0 & 0 \\ 0 & 1 & 0 & 0 & -1 & 0 \\ 1 & 1 & 1 & 0 & 0 & 0 \\ 0 & 0 & 0 & 1 & 1 & 1 \end{bmatrix}, \quad \mathbf{a}(e) = \frac{1}{6} \begin{bmatrix} 3 & 0 & -3 & -3 & 0 & 3 \\ 0 & 3 & -3 & 0 & -3 & 3 \\ 1 & 1 & 4 & 1 & 1 & -2 \\ 1 & 1 & -2 & 1 & 1 & 4 \end{bmatrix}, \quad (3.32)$$

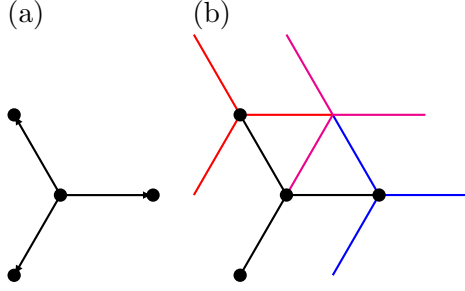


Figure 3.9: Building block of the triangular lattice, and its translations by  $B = \{\beta_1, \beta_2\}$ . (a) building block  $\{b\}$  of the triangular lattice, (b) the blue, red, and magenta blocks are the block translated by  $\beta_1$ ,  $\beta_2$ , and  $\beta_1 + \beta_2$ .

$$\begin{aligned}
e_1^{\max} &= (1/6)(3\alpha_1 + \alpha_3 + \alpha_4), \\
e_2^{\max} &= (1/6)(3\alpha_2 + \alpha_3 + \alpha_4), \\
e_3^{\max} &= (1/6)(-3\alpha_1 - 3\alpha_2 + 4\alpha_3 - 2\alpha_4), \\
e_4^{\max} &= (1/6)(-3\alpha_1 + \alpha_3 + \alpha_4), \\
e_5^{\max} &= (1/6)(-3\alpha_2 + \alpha_3 + \alpha_4), \\
e_6^{\max} &= (1/6)(3\alpha_1 + 3\alpha_2 - 2\alpha_3 + 4\alpha_4),
\end{aligned} \tag{3.33}$$

By (3.28) and (3.33), we obtain

$$\begin{aligned}
e_1 &= (1/2)\beta_1, & e_2 &= (1/2)\beta_2, & e_3 &= -(1/2)(\beta_1 + \beta_2), \\
e_4 &= -(1/2)\beta_1, & e_5 &= -(1/2)\beta_2, & e_6 &= (1/2)(\beta_1 + \beta_2),
\end{aligned} \tag{3.34}$$

and by (3.27) and (3.34), we also obtain

$$B = [\langle \beta_i, \beta_j \rangle] = \begin{bmatrix} 2 & 0 \\ 0 & 2 \end{bmatrix} - \begin{bmatrix} 1 & -1 \\ 1 & -1 \end{bmatrix} \begin{bmatrix} 1/3 & 0 \\ 0 & 1/3 \end{bmatrix} \begin{bmatrix} 1 & 1 \\ -1 & -1 \end{bmatrix} = \frac{2}{3} \begin{bmatrix} 2 & -1 \\ -1 & 2 \end{bmatrix}$$

On the other hand, the shortest paths from  $\mathbf{v}_0$  to other vertices are

$$\text{spath}(\mathbf{v}_0, \mathbf{v}_i) = (\mathbf{v}_0 \mathbf{v}_i) = e_i \quad \text{spath}(\mathbf{v}_0, \mathbf{w}_i) = (\mathbf{v}_0 \mathbf{w}_i) = e_{i+3} \quad i = 1, 2, 3.$$

By using the Cholesky decomposition, we may write

$$\begin{bmatrix} \beta_1 \\ \beta_2 \end{bmatrix} = \begin{bmatrix} 2/\sqrt{3} & -1/\sqrt{3} \\ 0 & 1 \end{bmatrix},$$

and hence by (3.34), we obtain

$$e_1 = -e_4 = \begin{bmatrix} 1/\sqrt{3} \\ 0 \end{bmatrix}, \quad e_2 = -e_5 = \begin{bmatrix} -1/(2\sqrt{3}) \\ 1/2 \end{bmatrix}, \quad e_3 = -e_6 = \begin{bmatrix} 1/(2\sqrt{3}) \\ 1/2 \end{bmatrix},$$

and

$$\begin{aligned}
\mathbf{v}_0 &= \begin{bmatrix} 0 \\ 0 \end{bmatrix}, & \mathbf{v}_1 &= \mathbf{v}_0 + e_1 = \begin{bmatrix} 1/\sqrt{3} \\ 0 \end{bmatrix}, & \mathbf{v}_2 &= \mathbf{v}_0 + e_2 = \begin{bmatrix} -1/(2\sqrt{3}) \\ 1/2 \end{bmatrix}, \\
\mathbf{w}_1 &= \mathbf{v}_0 + e_4 = \begin{bmatrix} -1/\sqrt{3} \\ 0 \end{bmatrix}, & \mathbf{w}_2 &= \mathbf{v}_0 + e_5 = \begin{bmatrix} 1/(2\sqrt{3}) \\ -1/2 \end{bmatrix}.
\end{aligned}$$

The above datas allow us to write figure in Fig. 3.1 (d) (see also Fig. 3.10). Since  $\Delta \mathbf{v}_0 \mathbf{v}_1 \mathbf{v}_2$  and  $\Delta \mathbf{v}_0 \mathbf{w}_1 \mathbf{w}_2$  consist regular triangles, a standard realization of kagome lattices is consisted by regular triangles sharing vertices each other.

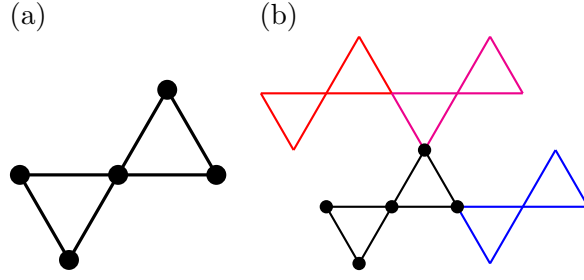


Figure 3.10: Building block of the kagome lattice, and its translations by  $B = \{\beta_1, \beta_2\}$ . (a) building block  $\{b\}$  of the triangular lattice, (b) the blue, red, and magenta blocks are blocks translated by  $\beta_1$ ,  $\beta_2$ , and  $\beta_1 + \beta_2$ .

Next, we consider higher dimensional analogues of kagome lattices. As mentioned in Example 3.38, a standard realization of a kagome lattice consists by regular triangles sharing vertices each other. One of the 3-dimensional analogues of kagome lattices is a hyper-kagome lattice of type II, whose standard realization consists quadrilaterals sharing vertices each other. Since a triangles in  $\mathbb{R}^2$  is a 1-simplex, the other is a hyper-kagome lattice of type I, whose standard realization consists 1-skeleton of 2-simplex sharing vertices each other.

**Example 3.39 (3D kagome lattice of type I, Sunada [39, Section 8.3]).** One of the 3-dimensional analogues of kagome lattices is defined as follows. Let  $X_0$  be a graph in Fig. 3.11 (b), and  $\tilde{X}$  be its maximal abelian covering. Since  $b = \text{rank } H_1(X_0, \mathbb{R}) = 9$ ,  $\tilde{X}$  is 9-dimensional a topological crystal. Take a  $\mathbb{Z}$ -basis of  $H_1(X_0, \mathbb{R})$  as

$$\begin{aligned} \alpha_1 &= e_1 - e_4, & \alpha_2 &= e_2 - e_5, & \alpha_3 &= e_3 - e_6, \\ \alpha_4 &= e_7 - e_2 + e_1, & \alpha_5 &= e_8 - e_3 + e_2, & \alpha_6 &= e_9 - e_1 + e_3, \\ \alpha_7 &= e_{10} + e_5 - e_4, & \alpha_8 &= e_{11} + e_6 - e_5, & \alpha_9 &= e_{12} + e_4 - e_6, \end{aligned}$$

and

$$H = \text{span}\{\alpha_4, \alpha_5, \alpha_6, \alpha_7, \alpha_8, \alpha_9\}.$$

The number of vertices in a building block in  $H_1(X_0, \mathbb{R})$  is 7, and the shortest paths from  $v_0$  are

$$\begin{aligned} \text{spath}(v_0, v_1) &= e_1, & \text{spath}(v_0, v_2) &= e_2, & \text{spath}(v_0, v_3) &= e_3, \\ \text{spath}(v_0, w_1) &= -e_4, & \text{spath}(v_0, w_2) &= -e_5, & \text{spath}(v_0, w_3) &= -e_6. \end{aligned}$$

A building block are

$$\begin{aligned} e_1 &= \begin{bmatrix} 1/2 \\ 0 \\ 0 \end{bmatrix}, & e_2 &= \begin{bmatrix} 1/4 \\ \sqrt{3}/4 \\ 0 \end{bmatrix}, & e_3 &= \begin{bmatrix} 1/4 \\ 1/(4\sqrt{3}) \\ 1/\sqrt{6} \end{bmatrix}, & e_4 &= \begin{bmatrix} -1/2 \\ 0 \\ 0 \end{bmatrix} \\ e_5 &= \begin{bmatrix} -1/4 \\ -\sqrt{3}/4 \\ 0 \end{bmatrix}, & e_6 &= \begin{bmatrix} -1/4 \\ -1/(4\sqrt{3}) \\ -1/\sqrt{6} \end{bmatrix}, & e_7 &= \begin{bmatrix} -1/4 \\ \sqrt{3}/4 \\ 0 \end{bmatrix}, & e_8 &= \begin{bmatrix} 0 \\ -1/(2\sqrt{3}) \\ 1/\sqrt{6} \end{bmatrix} \\ e_9 &= \begin{bmatrix} 1/4 \\ -1/(4\sqrt{3}) \\ -1/\sqrt{6} \end{bmatrix}, & e_{10} &= \begin{bmatrix} -1/4 \\ \sqrt{3}/4 \\ 0 \end{bmatrix}, & e_{11} &= \begin{bmatrix} 0 \\ -1/(2\sqrt{3}) \\ 1/\sqrt{6} \end{bmatrix}, & e_{12} &= \begin{bmatrix} 1/4 \\ -1/(4\sqrt{3}) \\ -1/\sqrt{6} \end{bmatrix} \end{aligned}$$

and

$$\begin{bmatrix} \beta_1 \\ \beta_2 \\ \beta_3 \end{bmatrix} = \begin{bmatrix} 1 & 0 & 0 \\ 1/2 & \sqrt{3}/2 & 0 \\ 1/2 & 1/(2\sqrt{3}) & \sqrt{2/3} \end{bmatrix},$$

then we obtain 3D kagome lattice of type I (Fig. 3.12). This lattice is sometimes called as *Pyrochlore lattice* or simply *hyper-kagome lattice*.

**Example 3.40 (3D kagome lattice of type II, Sunada [39, Section 8.3]).** The other 3-dimensional analogue of kagome lattices is defined as follows. Let  $X_0$  be a graph in Fig. 3.11 (c), and  $\tilde{X}$  be its maximal abelian covering. Since  $b = \text{rank } H_1(X_0, \mathbb{R}) = 5$ ,  $\tilde{X}$  is 5-dimensional a topological crystal. Take a  $\mathbb{Z}$ -basis of  $H_1(X_0, \mathbb{R})$  as

$$\begin{aligned}\alpha_1 &= e_1 - e_4, & \alpha_2 &= e_2 - e_5, & \alpha_3 &= e_3 - e_6, \\ \alpha_4 &= e_1 + e_2 + e_3 + e_4, & \alpha_5 &= e_5 + e_6 + e_7 + e_8,\end{aligned}$$

and

$$H = \text{span}\{e_1 + e_2 + e_3 + e_4, e_5 + e_6 + e_7 + e_8\}.$$

The number of vertices in a building block in  $H_1(X_0, \mathbb{R})$  is 7, and the shortest paths from  $v_0$  are

$$\begin{aligned}\text{spath}(v_0, v_1) &= e_1, & \text{spath}(v_0, v_2) &= e_1 + e_2, & \text{spath}(v_0, v_3) &= e_1 + e_2 + e_3, \\ \text{spath}(v_0, w_1) &= e_5, & \text{spath}(v_0, w_2) &= e_5 + e_6, & \text{spath}(v_0, w_3) &= e_5 + e_6 + e_7.\end{aligned}$$

A building block are

$$\begin{aligned}e_1 &= \begin{bmatrix} (1/2)\sqrt{3/2} \\ 0 \\ 0 \end{bmatrix}, & e_2 &= \begin{bmatrix} -1/(2\sqrt{6}) \\ 1/\sqrt{3} \\ 0 \end{bmatrix}, & e_3 &= \begin{bmatrix} -1/(2\sqrt{6}) \\ -1/(2\sqrt{3}) \\ 1/2 \end{bmatrix}, & e_4 &= \begin{bmatrix} -1/(2\sqrt{6}) \\ -1/(2\sqrt{3}) \\ -1/2 \end{bmatrix} \\ e_5 &= \begin{bmatrix} -(1/2)\sqrt{3/2} \\ 0 \\ 0 \end{bmatrix}, & e_6 &= \begin{bmatrix} 1/(2\sqrt{6}) \\ -1/\sqrt{3} \\ 0 \end{bmatrix}, & e_7 &= \begin{bmatrix} 1/(2\sqrt{6}) \\ 1/(2\sqrt{3}) \\ -1/2 \end{bmatrix}, & e_8 &= \begin{bmatrix} 1/(2\sqrt{6}) \\ 1/(2\sqrt{3}) \\ 1/2 \end{bmatrix},\end{aligned}$$

and

$$\begin{bmatrix} \beta_1 \\ \beta_2 \\ \beta_3 \end{bmatrix} = \begin{bmatrix} \sqrt{3/2} & -1/\sqrt{6} & -1/\sqrt{6} \\ 0 & 2/\sqrt{3} & -1/\sqrt{3} \\ 0 & 0 & 1 \end{bmatrix},$$

then we obtain 3D kagome lattice of type II (Fig. 3.13).

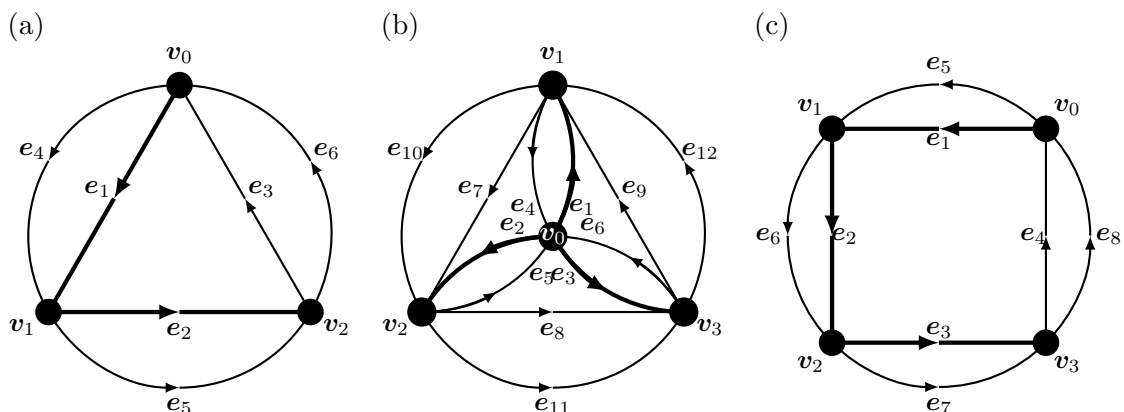


Figure 3.11: (a) The base graph of kagome lattices, (b) the base graph of 3D kagome lattices of type I, (c) the base graph of 3D kagome lattices of type II.

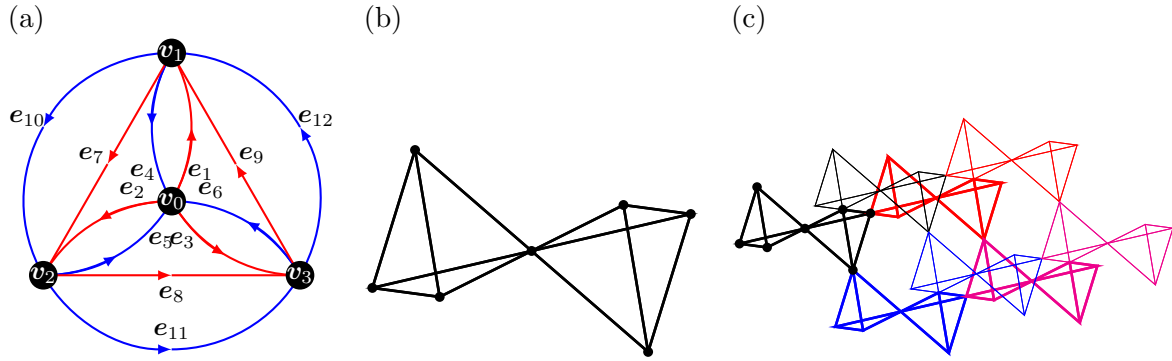


Figure 3.12: Building block of the 3D kagome lattice of type I, and its translations by  $B = \{\beta_1, \beta_2, \beta_3\}$ . (a) Each graph consisted by blue edges with vertices and by red edges with vertices is a tetrahedral graph. (b) building block  $\{\mathbf{b}\}$ , (c) the blue, red, and magenta blocks are blocks translated by  $\beta_1$ ,  $\beta_2$ , and  $\beta_1 + \beta_2$ . The thin layer are translated by  $\beta_3$  of above them.

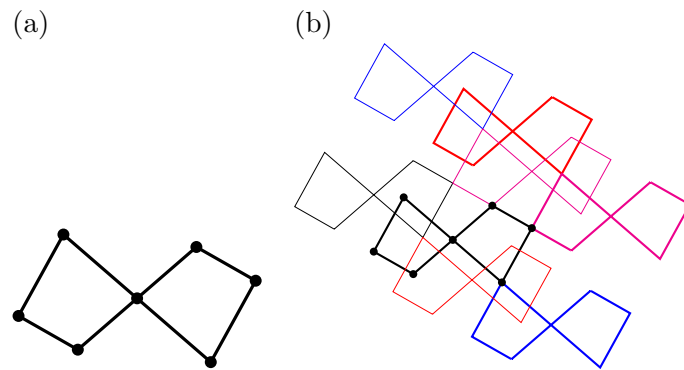


Figure 3.13: Building block of the 3D kagome lattice of type II, and its translations by  $B = \{\beta_1, \beta_2, \beta_3\}$ . (a) building block  $\{\mathbf{b}\}$ , (b) the blue, red, and magenta blocks are blocks translated by  $\beta_1$ ,  $\beta_2$ , and  $\beta_1 + \beta_2$ . The thin layer are translated by  $\beta_3$  of above them.



**Example 3.41 (Cairo pentagonal tiling, Sunada [39, Section 8.3]).** A periodic tessellations is also considered as a topological crystal. A Cairo pentagonal tiling (Fig. 3.14 (b)) is a tessellation by congruent pentagons, and it is topologically equivalent to the basketweave tiling (Fig. 3.14 (a)). It is also called MacMahon's net [30]. Here, we compute a standard realization of the cairo pentagonal tiling.

We number vertices and edges of the graph of a fundamental region of the basketweave tiling as Fig. 3.14 (a). Taking a basis  $\{\mathbf{p}_1, \mathbf{p}_2\}$  of the period lattice, then we obtain the equation of harmonic realizations (the equation of the balancing condition) as

$$\begin{aligned}
4\mathbf{v}_0 &= \mathbf{v}_2 + (\mathbf{v}_9 - \mathbf{p}_2) + (\mathbf{v}_4 - \mathbf{p}_1) + (\mathbf{v}_{11} - \mathbf{p}_1 - \mathbf{p}_2), & 4\mathbf{v}_1 &= \mathbf{v}_3 + \mathbf{v}_4 + (\mathbf{v}_9 - \mathbf{p}_2) + (\mathbf{v}_{10} - \mathbf{p}_2), \\
3\mathbf{v}_2 &= \mathbf{v}_0 + \mathbf{v}_3 + \mathbf{v}_6, & 3\mathbf{v}_3 &= \mathbf{v}_1 + \mathbf{v}_2 + \mathbf{v}_7, \\
3\mathbf{v}_4 &= \mathbf{v}_1 + \mathbf{v}_5 + (\mathbf{v}_0 + \mathbf{p}_1), & 3\mathbf{v}_5 &= \mathbf{v}_7 + \mathbf{v}_4 + (\mathbf{v}_6 + \mathbf{p}_1), \\
4\mathbf{v}_6 &= \mathbf{v}_2 + \mathbf{v}_8 + (\mathbf{v}_5 - \mathbf{p}_1) + (\mathbf{v}_{11} - \mathbf{p}_1), & 4\mathbf{v}_7 &= \mathbf{v}_3 + \mathbf{v}_5 + \mathbf{v}_8 + \mathbf{v}_{10}, \\
3\mathbf{v}_8 &= \mathbf{v}_6 + \mathbf{v}_7 + \mathbf{v}_9, & 3\mathbf{v}_9 &= \mathbf{v}_8 + \mathbf{v}_0 + \mathbf{p}_2 + \mathbf{v}_1 + \mathbf{p}_2, \\
3\mathbf{v}_{10} &= \mathbf{v}_7 + \mathbf{v}_1 + \mathbf{p}_2 + \mathbf{v}_{11}, & 3\mathbf{v}_{11} &= \mathbf{v}_{10} + \mathbf{v}_6 + \mathbf{p}_1 + \mathbf{v}_0 + \mathbf{p}_1 + \mathbf{p}_2.
\end{aligned} \tag{3.35}$$

For a given basis  $\{\mathbf{p}_1, \mathbf{p}_2\}$ , we obtain a solution of (3.35) (a harmonic realization of the cairo pentagonal tiling) as

$$\begin{aligned}
\mathbf{v}_0 &= \mathbf{0}, & \mathbf{v}_1 &= (1/2)\mathbf{p}_1, & \mathbf{v}_2 &= (1/8)(\mathbf{p}_1 + 2\mathbf{p}_2), \\
\mathbf{v}_3 &= (1/8)(3\mathbf{p}_1 + 2\mathbf{p}_2), & \mathbf{v}_4 &= (1/8)(6\mathbf{p}_1 + \mathbf{p}_2), & \mathbf{v}_5 &= (1/8)(6\mathbf{p}_1 + 3\mathbf{p}_2), \\
\mathbf{v}_6 &= (1/2)\mathbf{p}_2, & \mathbf{v}_7 &= (1/8)(4\mathbf{p}_1 + 4\mathbf{p}_2), & \mathbf{v}_8 &= (1/8)(2\mathbf{p}_1 + 5\mathbf{p}_2), \\
\mathbf{v}_9 &= (1/8)(2\mathbf{p}_1 + 7\mathbf{p}_2), & \mathbf{v}_{10} &= (1/8)(5\mathbf{p}_1 + 6\mathbf{p}_2), & \mathbf{v}_{11} &= (1/8)(7\mathbf{p}_1 + 6\mathbf{p}_2).
\end{aligned} \tag{3.36}$$

A harmonic realization (3.36) is standard if and only if  $\{e_i\}_{i=1}^{20}$  satisfies (3.6). Taking  $\mathbf{f}_1 = (1, 0)^T$  and  $\mathbf{f}_2 = (0, 1)^T$ , and solving

$$\sum_{i=1}^{20} \langle e_i, \mathbf{f}_j \rangle e_i = c\mathbf{f}_j, \quad j = 1, 2, \tag{3.37}$$

then we obtain

$$|\mathbf{p}_1| = |\mathbf{p}_2|, \quad \langle \mathbf{p}_1, \mathbf{p}_2 \rangle = 0. \tag{3.38}$$

Substituting (3.38) into (3.36), we obtain a standard realization of a Cairo pentagonal tiling (Fig. 3.14 (b) and Fig. 3.15 (c)).

**Remark 3.42.** The carbon structure with regular hexagonal shaped is called a graphene (see Section 3.3), and the carbon structure with a Cairo pentagonal shaped is called a penta-graphene [43].

**Remark 3.43.** A Cairo pentagonal tiling is constructed by line segments joining four vertices of a square as in Fig. 3.16 (a) and (b). Define three kind of energies  $L$ ,  $E$  and  $C$  by

$$\begin{aligned}
L(t) &= |\mathbf{a} - \boldsymbol{\alpha}| + |\mathbf{b} - \boldsymbol{\alpha}| + |\mathbf{c} - \boldsymbol{\beta}| + |\mathbf{d} - \boldsymbol{\beta}| + |\boldsymbol{\alpha} - \boldsymbol{\beta}| = 1 - 2t + 2\sqrt{1 + 4t^2}, \\
E(t) &= |\mathbf{a} - \boldsymbol{\alpha}|^2 + |\mathbf{b} - \boldsymbol{\alpha}|^2 + |\mathbf{c} - \boldsymbol{\beta}|^2 + |\mathbf{d} - \boldsymbol{\beta}|^2 + |\boldsymbol{\alpha} - \boldsymbol{\beta}|^2 = 8t^2 - 4t + 2, \\
C(t) &= |\mathbf{a} - \boldsymbol{\alpha}|^{-1} + |\mathbf{b} - \boldsymbol{\alpha}|^{-1} + |\mathbf{c} - \boldsymbol{\beta}|^{-1} + |\mathbf{d} - \boldsymbol{\beta}|^{-1} + |\boldsymbol{\alpha} - \boldsymbol{\beta}|^{-1}.
\end{aligned}$$

For each  $t \in (-1/2, 1/2)$ , the configuration in Fig. 3.16 (b) yields a monohedral pentagon tiling. The energy  $L$  attains its minimum at  $t = 1/(2\sqrt{3})$ , and then the angle  $\theta = \theta(t)$  in Fig. 3.16

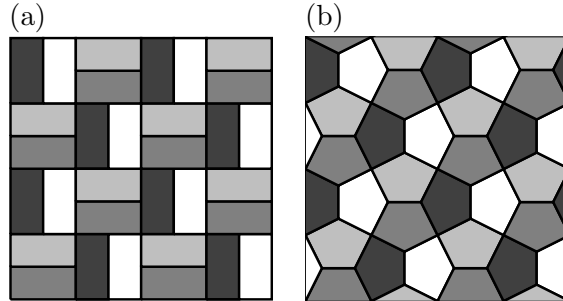


Figure 3.14: (a) A basketweave tiling, (b) a Cairo tiling. Both 1-skeletons of the tiling are topologically equivalent.

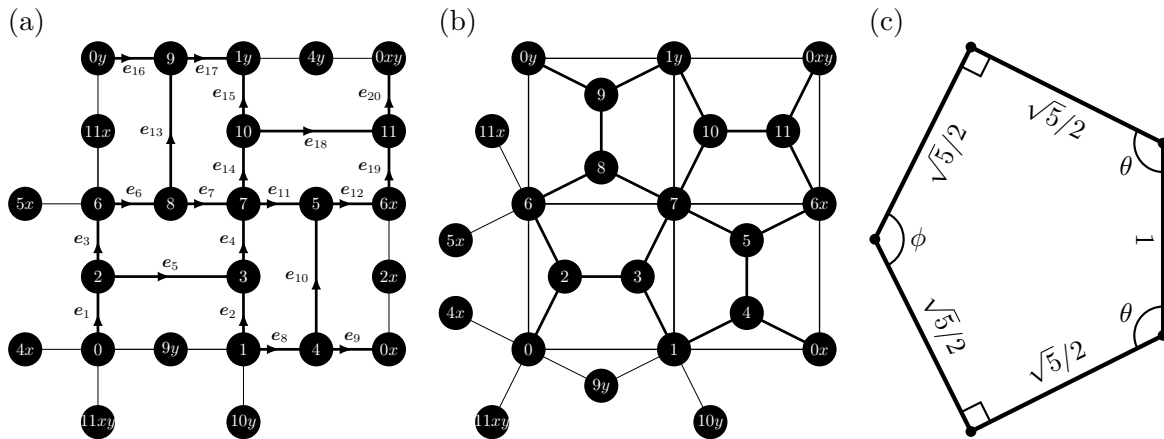


Figure 3.15: (a) Numbering of vertices and edges of a fundamental region of the basketweave tiling, (b) a fundamental region of a standard realization of the Cairo tiling, (c) the congruent-pentagon of the standard realization. The ratio of length of edges is  $1 : (\sqrt{5}/2)$ , and angles are  $\cos(\theta) = -1/\sqrt{5}$  and  $\cos(\phi) = -3/5$  ( $\theta \sim 116.57^\circ$  and  $\phi \sim 126.87^\circ$ ).

(a) satisfies  $\cos(\theta) = -1/2$ , ( $\theta = 2\pi/3$ ). The minimum of  $L$  gives us the configuration of the minimum length of line segments, On the other hand, the energy  $E$  attains its minimum at  $t = 1/4$ , and then the angle  $\theta$  satisfies  $\cos(\theta) = -1/\sqrt{5}$ . The minimum of  $E$  gives us a standard realization of the Cairo pentagonal tiling (see also Fig. 3.15 (c)). The energy  $C$  is based on the Coulomb repulsive force, and attains its local minimum at  $t \sim 0.17264$ , the angle  $\theta$  satisfies  $\cos(\theta) \sim -0.326374$ .

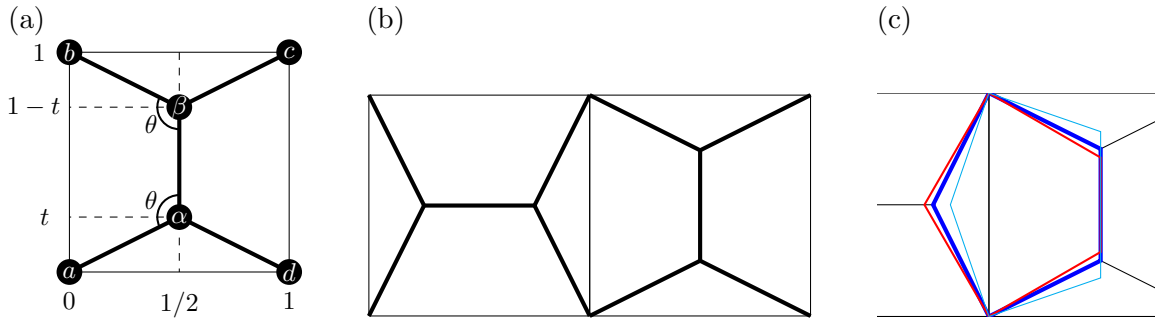


Figure 3.16: (a) Move  $\alpha$  and  $\beta$  on the line  $x = 1/2$ , and calculate minimum of  $L(t)$  and  $E(t)$ , (b) a building block of the pentagonal tiling, (c) the red, blue, and cyan pentagons are minimizers of  $L$ ,  $E$  and  $C$ , respectively.

**Remark 3.44.** This algorithm is easily programmable by using Kruskal's and Dijkstra's algorithms, and the Cholesky decomposition. To calculate the matrix  $A$  and vectors  $a(e)$ ,  $b(e)$ , it is easy to set  $e_i = (0, \dots, 1, \dots, 0) \in \mathbb{R}^{|E|}$ .

**Example 3.45.** By using Mathematica, coordinates of vertices of standard realizations of topological crystals are easy to compute, if we obtain a  $\mathbb{Z}$ -basis of  $H_1(X_0, \mathbb{Z})$  and a  $\mathbb{Z}$ -basis of vanishing subspace  $H$  (and a spanning tree of  $X_0$ ). The following is a sample code of Mathematica to compute vertices of a kagome lattice (lines 1 and 3 are specific datas of a kagome lattice).

```

numberOfEdges=6;b=4;d=2;
e = IdentityMatrix[numberOfEdges];
alpha = {e[[1]]-e[[4]], e[[2]]-e[[5]], e[[1]]+e[[2]]+e[[3]],
e[[4]]+e[[5]]+e[[6]]};
matrixA = alpha.Transpose[alpha];
matrixb = Table[e[[j]].alpha[[i]], {i, 1, b}, {j, 1, numberOfEdges}];
matrixa = Inverse[matrixA].matrixb;
matrixA11 = matrixA[[1;;d,1;;d]]; matrixA22 = matrixA[[d+1;;b,d+1;;b]];
matrixA12 = matrixA[[1;;d,d+1;;b]]; matrixA21 = matrixA[[d+1;;b,1;;d]];
matrixB = matrixA11 - matrixA12.Inverse[matrixA22].matrixA21;
matrixprojecta = matrixa[[1;;d]];
beta = CholeskyDecomposition[matrixB];
beta.matrixprojecta

```

The output of this code is

$$\begin{bmatrix} 1/\sqrt{3} & -1/(2\sqrt{3}) & -1/(2\sqrt{3}) & -1/\sqrt{3} & 1/(2\sqrt{3}) & 1/(2\sqrt{3}) \\ 0 & 1/2 & -1/2 & 0 & -1/2 & 1/2 \end{bmatrix},$$

which expresses coordinates of vertices of a kagome lattice. To obtain complete datas of standard realizations, we should obtain datas of building blocks by using datas of the shortest paths from an origin.

**Remark 3.46.** Crystallographers often call periodic realizations in  $\mathbb{R}^2$  and  $\mathbb{R}^3$  of graphs *2-net* and *3-net*, respectively. Names of 2-net of each lattice are

<b>sq1</b>	the regular square lattice,
<b>hcb</b>	the regular hexagonal lattice (honeycomb lattice)
<b>hx1</b>	the regular triangular lattice
<b>kgm</b>	the regular kagome lattice,
<b>mcm</b>	the 1-skeleton of Cairo pentagonal tiling,

and names of 3-net of each lattice are

<b>pcu</b>	the regular cubic lattice,
<b>dia</b>	the diamond lattice,
<b>src</b>	the gyroid lattice,
<b>crs</b>	the 3D kagome lattice of type I,
<b>lvt</b>	the 3D kagome lattice of type II.

Lists of 2-net and 3-net are available in EPINET [2].

### 3.3 Carbon structures and standard realizations

In this section, we consider carbon crystal structures via standard realizations.

Graphene is an allotrope of carbons, and is 2-dimensional crystal structure. Each carbon atom binds chemically other three carbon atoms by  $sp^2$ -orbitals (see Fig. 3.17). In mathematical view points, a graphene is a standard realization of a regular hexagonal lattice. A fundamental piece (Fig. 3.17) is a graph with four points, where each point locates at vertices of regular triangle and its barycenter. Translating the fundamental piece by  $\alpha_1$  and  $\alpha_2$  with  $|\alpha_i| = 1$  and  $\langle \alpha_1, \alpha_2 \rangle = (1/2)|\alpha_1||\alpha_2|$ , we obtain a structure of graphenes.

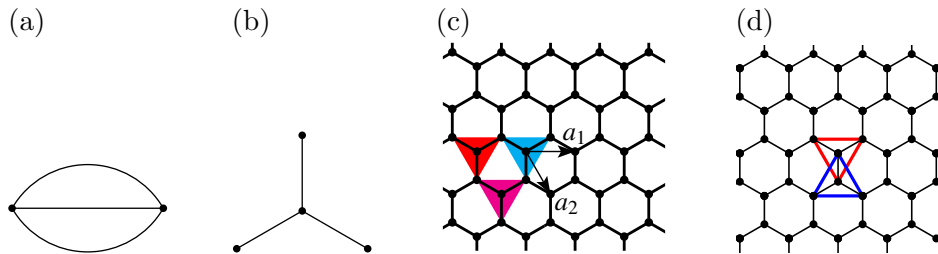


Figure 3.17: (a) The base graph of a regular hexagonal lattice, (b) a fundamental piece of a regular hexagonal lattice, (c) a graphene structure, which is constructed by (b) and its translations, (d) the barycenter of the blue regular triangle is a vertex of the red regular triangle. The blue triangle is consisted by  $w_1$ ,  $w_2$ , and  $w_3$  (by using notations in Example 3.32), then the red is consisted by  $v_0$ ,  $v_0 + \alpha_1$ , and  $v_0 + \alpha_1 - \alpha_2$ . The barycenters of blue and red are  $v_0$  and  $w_1$ , respectively.

Diamond is also an allotrope of carbons, and is 3-dimensional crystal structure. Each carbon atom binds chemically other four carbon atoms by  $sp^3$ -orbitals (see Fig. 3.18). In mathematical view points, a diamond is a standard realization of a graph, which can be called regular tetrahedral graph. A fundamental piece (Fig. 3.18) is a graph with five points, each points located at vertices of regular tetrahedron and its barycenter. Translating the fundamental piece by  $\alpha_1$ ,  $\alpha_2$ , and  $\alpha_3$  with  $|\alpha_i| = 1$  and  $\langle \alpha_i, \alpha_j \rangle = (1/3)|\alpha_i||\alpha_j|$  if  $i \neq j$ , we obtain a structure of diamonds.

By a textbook of physical chemistry, the space group of diamond structure is  $Fd\bar{3}m$ , which expresses face-centered structure with a glide reflection, three improper rotations, and certain

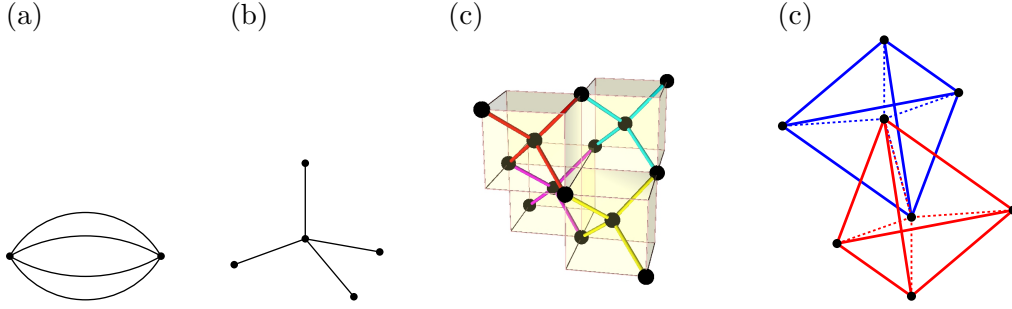


Figure 3.18: (a) The base graph of a diamond structure, (b) a fundamental piece of a diamond structure, whose vertices are located at vertices of a regular tetrahedron and its barycenter, (c) a diamond structure. A diamond structure is constructed by (b) and its translations. (d) the barycenter of the blue regular tetrahedron is a vertex of the red regular tetrahedron. The blue tetrahedron is consisted by  $v_1, v_2, v_3,$  and  $v_4$  (by using notations in Example 3.33), then the red is consisted by  $v_0, w_1 - w_2 = v_0 + \alpha_1 - \alpha_2, w_1 - w_3 = v_0 + \alpha_1 - \alpha_3,$  and  $v_0 + w_1 - w_4 = v_0 + \alpha_1.$  The barycenters of blue and red are  $v_0$  and  $w_1,$  respectively.

reflections. Diamond structures are constructed shown in Fig. 3.19; however it is difficult to realize for mathematicians. On the other hand, the construction diamond structures by standard realizations is easy for mathematicians.

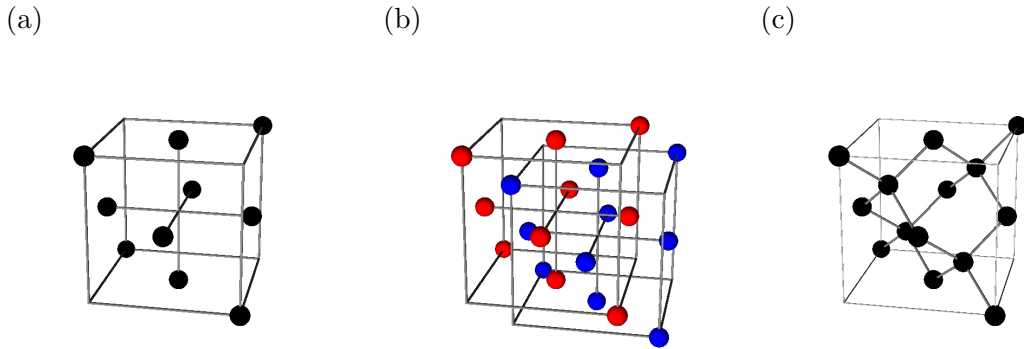


Figure 3.19: How to construct a diamond structure: (a) prepare a face-centered structure, (b) duplicate it and translate to a diagonal direction, and then (c) we obtain a diamond structure.

$K_4$  structures are obtained by standard realizations of the  $K_4$  graph. The  $K_4$  graph is the complete graph with four vertices (each vertex connects to all other vertices). Each carbon atom of  $K_4$  structures binds chemically other three atoms by  $sp^2$ -orbitals (see Fig. 3.20). A fundamental piece is a graph with seven points. Translation vectors  $\{\alpha_i\}_{i=1}^3$  satisfy  $|\alpha_i| = 1$  and  $\langle \alpha_i, \alpha_j \rangle = -(1/3)|\alpha_i||\alpha_j|$  ( $i \neq j$ ). Moreover,  $K_4$  structures have chirality, that is, A  $K_4$  structure and its mirror image are not same.

Physical property of the  $K_4$  carbon is computed by Itoh–Kotani–Naito–Sunada–Kawazoe–Adschiri [13], it is physically meta-stable and metallic; however it has not composed yet. Recently, Mizuno–Shuku–Matsushita–Tsuchiizu–Hara–Wada–Shimizu–Awaga compose a  $K_4$  structure other than carbons [27]. Their structure is a molecular- $K_4$ , a radical molecule NDI- $\Delta(-)$  consists a  $K_4$  crystal.

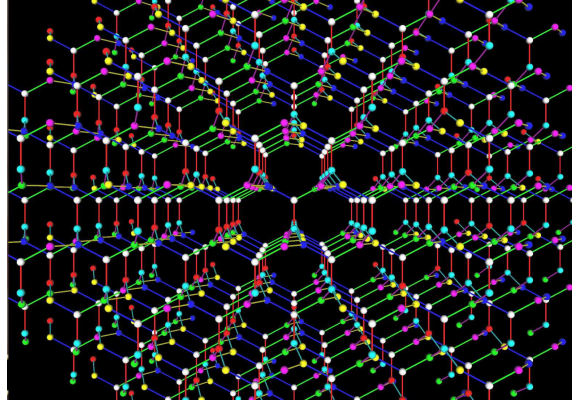


Figure 3.20: A  $K_4$  structure, this is the image of the cover page of Notices Amer. Math. Soc., **55**, drawn by the author.

## 4 Negatively curved carbon structures

### 4.1 Carbon structures as discrete surfaces

In 1990's, several new  $sp^2$ -carbon structures, fullerenes (including  $C_{60}$ ), graphene, and carbon nanotubes were found (See Fig. 4.1). These structures look like surfaces in  $\mathbb{R}^3$ . For example,

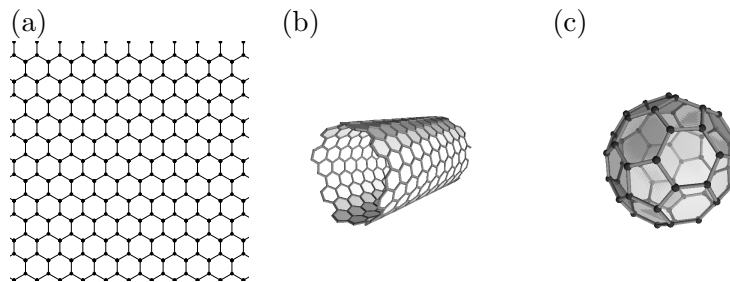


Figure 4.1: (a) Graphene, (b) (single wall) carbon nanotube, (c)  $C_{60}$  (an example of fullerenes).

a graphene,  $C_{60}$ , and a nanotube are similar to a plane, a sphere, and a cylinder, respectively. Each continuous surface in the above has non-negatively curved, i. e., the Gauss curvature of a sphere is positive, and theses of a cylinder and plane are zero. Hence, it is a natural question if an  $sp^2$ -carbon structure which looks like a negatively curved surface exists or not.

In the followings, we consider  $sp^2$ -carbon structures as “trivalent discrete surface” (realizations of 3-regular graphs in  $\mathbb{R}^3$ ). Moreover, we assume that graphs are oriented surface graphs, that is, each graphs is realized on a oriented surface without self-intersections. By the property of surface graphs, we can define the notion of “faces” (simple closed path) for trivalent discrete surfaces.

**Definition 4.1.** For an oriented surface graph  $X = (V, E)$ , the *Euler number*  $\chi(X)$  of  $X$  is defined by

$$\chi(X) = |F| - |E| + |V|, \quad (4.1)$$

where  $|F|$  is the number of faces of  $X$ .

Note that the Euler number  $\chi(X)$  of an oriented graph  $X$  is same as the Euler number of the underlying surface.

**Proposition 4.2.** *Assume an oriented surface graph  $X = (V, E)$  is trivalent (3-regular) graph, then we obtain  $F = \sum N_k$ ,  $E = (1/2) \sum kN_k$ ,  $V = (1/3) \sum kN_k$ , where  $N_k$  is the number of  $k$ -gon in  $X$ . Hence, we also obtain*

$$\chi(X) = \sum (1 - k/6)N_k. \quad (4.2)$$

*Proof.* Since  $X$  is an oriented surface graph, each edges shared by two faces, and hence, we obtain  $|E| = (1/2) \sum kN_k$ . Since  $X$  is trivalent, each vertex shared by three faces, and hence, we obtain  $|V| = (1/3) \sum kN_k$ . Substituting them into (4.1), we obtain (4.2).  $\square$

**Remark 4.3.** By Proposition 4.2, the number of hexagons does not affect to the Euler number. If  $X$  is positively curved ( $\chi(X) > 0$ ), then at least one  $n$ -gon ( $n \leq 5$ ) should be contained in  $X$ . If  $X$  is negatively curved ( $\chi(X) < 0$ ), then at least one  $n$ -gon ( $n \geq 7$ ) should be contained in  $X$ .

	$N_5$	$N_6$	$N_7$	$N_8$	$ V $	$ E $	$ F $	$\chi$
$C_{60}$	12	20	0	0	60	90	32	2
SWNT $\mathbf{c} = (6, 6)$	0	12	0	0	24	36	12	0
Mackay–Terrones'	0	90	0	12	192	288	102	-4

Table 4.1: Number of polygons of  $C_{60}$ , a single-wall nanotube (of fundamental region of it), where  $\mathbf{c}$  is the chiral index of SWNT (see Section A.3), and Mackay–Terrones' structure (see Fig. 4.2 (b)).

By Proposition 4.2, if there exists an  $sp^2$ -carbon structure with  $\chi(X) < 0$  (negatively curved), then at least one  $n$ -gon ( $n \geq 7$ ) exists in  $X$ . In 1991, Mackay–Terrones [25] calculated an  $sp^2$ -carbon structure which is looked like a minimal surface (Schwarz P surface,  $\chi(X) = -4$ ), which contains 12 of octagons (see also Lenosky–Gonze–Teter–Elser [24]).

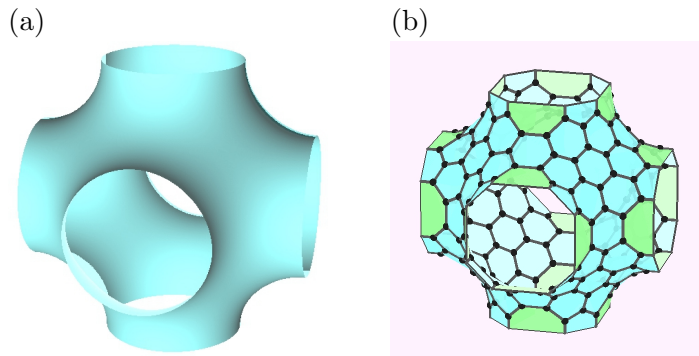


Figure 4.2: (a) Schwarz P surface, which is a triply periodic minimal surface (the Gauss curvature  $K < 0$ , the Euler number  $\chi = -4$ , and the genus  $g = -3$ ), whose period lattice  $\{\mathbf{e}_i\}_{i=1}^3$  satisfies  $\langle \mathbf{e}_i, \mathbf{e}_j \rangle = \delta_{ij}$ . (b) Mackay–Terrones' structure, the period lattice is the same as (a). Note that green faces in (b) are octagons (see also Table 4.1).

## 4.2 Construction of negatively curved carbon structures via standard realizations

Tagami–Liang–Naito–Kawazoe–Kotani [40] constructed negatively curved carbon crystals, which are different from the Mackay–Terrones' structure, by using standard realizations of topological crystals.

The fundamental region of Mackay–Terrones’ structure has octahedral symmetry, which is same symmetry of truncated octahedrons. Truncated octahedrons consist eight hexagons, which have  $D_6$ -symmetry (see 4.3). Our method is, 1) we classify and construct a graph in a

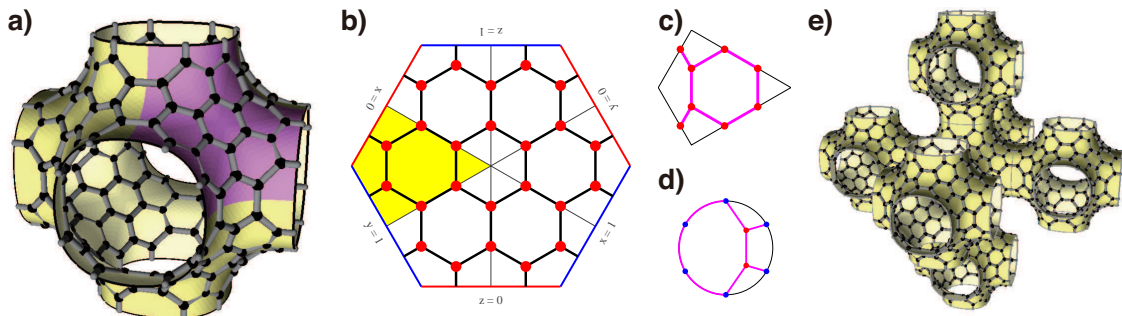


Figure 4.3: Symmetry of the Mackay–Terrones’ structure. (c) is a fundamental region of  $D_6$ -action on a hexagon, which is diffeomorphic to (d). See also Fig. A.5 (Tagami–Liang–Naito–Kawazoe–Kotani [40]).

fundamental region of  $D_6$ -action on a hexagon, which is a trivalent graph when we extend to hexagon by  $D_6$ -action (Fig. 4.3 (c)), 2) we extend the graph obtained in 1 to the trivalent graph on a hexagon (Fig. 4.3 (b)), 3) we extend the graph obtained in 2 to the graph on a truncated octahedron (Fig. 4.3 (a)), and 4) we calculate a standard realization of the graph obtained in 3. The structure obtained in 4 is a candidate of  $sp^2$ -carbon structure with  $K < 0$  ( $\chi = -4$ ). In fact, we prove the following result.

**Theorem 4.4** (Tagami–Liang–Naito–Kawazoe–Kotani [40]). *The equation to obtain standard realization is linear:  $\Delta \mathbf{x} = \mathbf{b}$ , where  $b_i = \pm e_\alpha$ , if a vertex  $v_i$  is adjacent to a vertex in neighbouring cell. The linear equation is solvable if and only if  $\sum b_i = 0$ . The period lattice  $\{\mathbf{e}_i\}$  which gives a standard realization is cubic, i. e.,  $\mathbf{e} = (\mathbf{e}_1, \mathbf{e}_2, \mathbf{e}_3)$  is a period lattice of a standard realization, then  $\mathbf{e}^T \mathbf{e} = \mathbf{E}$ . If  $\Phi$  is a standard realization, then  $\text{Aut}(X) \subset \text{Aut}(\Phi(X))$ , and hence  $X$  has the same symmetries with Mackay–Terrones’ structure.*

In our method, we do not solve the equation (3.6). Instead, we only solve the harmonic equation (3.3) using cubic periodicity. Hence, we should prove that the realization is standard. To prove it, we use the Lagrange multiplier, and the result of the Lagrange multiplier is  $\mathbf{e}^T \mathbf{e} = \mathbf{E}$ . This shows that the harmonic realizations with the cubic lattice is standard.

**Remark 4.5.** No negatively curved  $sp^2$ -carbon structure has been synthesised so far. However, a piece of negatively curved carbon structure is chemically synthesised by Kawasumi–Zhang–Segawa–Scott–Itami [15].

## 5 A discrete surface theory

In the previous section, we explain “negatively” curved carbon structure; however, the definition of negativity is that the Euler number is negative. This is a similar situation with that “a surface with genus  $\geq 2$  cannot be non-negatively curved”. Since the Gauss curvature of smooth surfaces is a function defined on each point of the surface, the negativity in the previous section is not a precise property for discrete surfaces.

On the other hand, there are many definitions of the Gauss curvature for discrete surfaces. One of the examples is a triangulation of a smooth surface, which is a discretization of a smooth



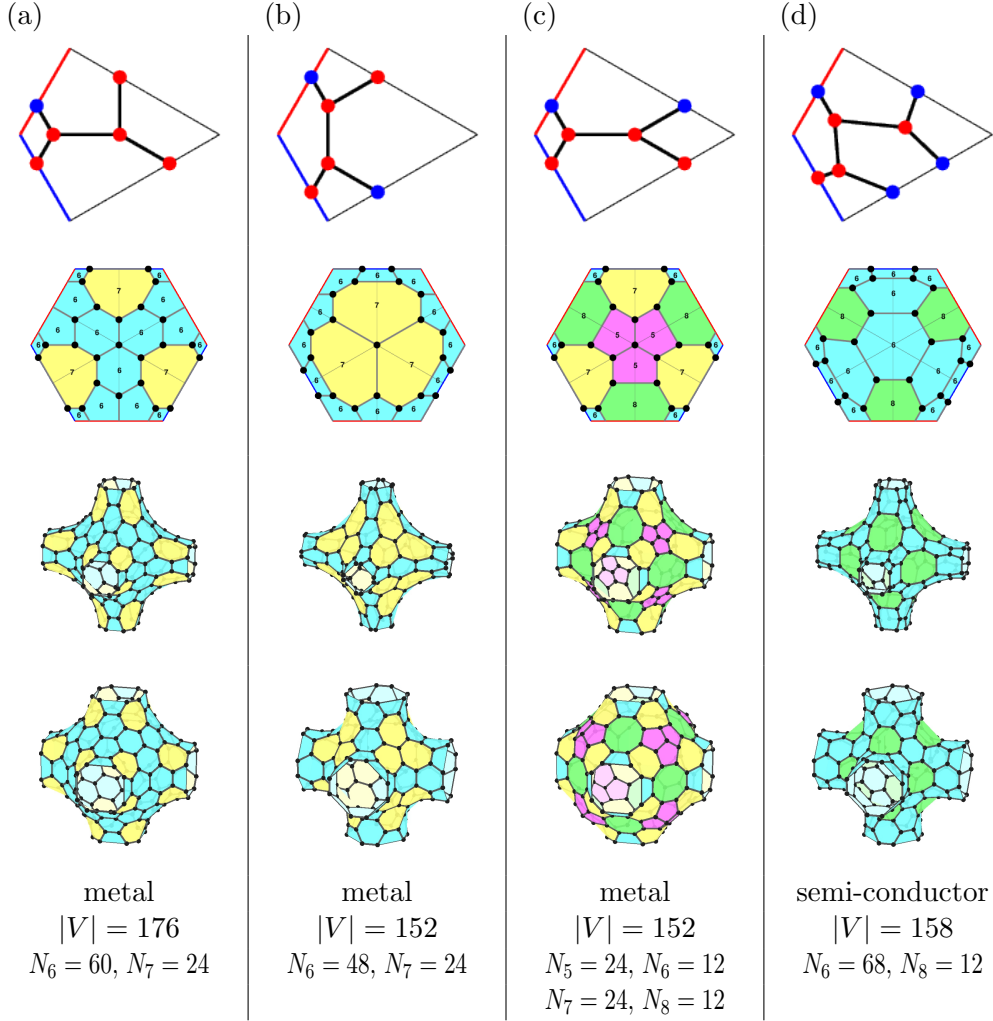


Figure 4.4: Mackay-like structures, which are physically stable. Physical stabilities are calculated by density functional theory (DFT). For the notion of “metal”/”semi-conductor”, see Section A.2. (Tagami–Liang–Naito–Kawazoe–Kotani [40]).

surface. For triangulation of smooth surfaces, the Gauss curvature is defined by “angle defects”, that is  $K(p) = 2\pi - \sum \theta_i$ , where  $\theta_i$  is inner angle at  $p$  of each triangle gathering at  $p$ .

Applying the definition of the Gauss curvature by angle defects to the Mackay–Terrones’ structure (a standard realization), we obtain  $K \equiv 0$ , since a standard realization of a trivalent topological crystal satisfies the “balance condition” (3.3), that is, each point and three neighbouring points are co-planer. Although each triangle of triangulations of smooth surfaces is planer, however, each face of the discrete surface is not planer.

Hence, we should construct a new definitions of the Gauss curvature and the mean curvature for trivalent discrete surfaces.

## 5.1 Curvatures of trivalent discrete surfaces

**Definition 5.1** (Kotani–Naito–Omori [16]). Let  $X = (V, E)$  be a trivalent graph, and  $\Phi: X \rightarrow \mathbb{R}^3$  be a realization of  $X$ . The realization  $\Phi$  is called a *trivalent discrete surface* if and only if for each  $x \in V$ , at least two vectors of  $\{\Phi(e) : e \in E_x\}$  are linearly independent.

We remark that this definition of trivalent discrete surfaces is not limited to topological

crystals, and thus we can treat  $C_{60}$  and single-wall nanotubes (SWNTs) for example. But, the definition also contains  $K_4$  structure as trivalent discrete surfaces, although, it does not look like a discrete surface.

Before giving a definition of curvatures for trivalent discrete surfaces, we recall properties of curvature for smooth surfaces in  $\mathbb{R}^2$ .

**Definition 5.2 (Curvatures for smooth surfaces).** Let  $p: \Omega \subset \mathbb{R}^2 \rightarrow \mathbb{R}^3$  be a smooth surface, and  $n(x)$  be a unit normal vector at  $x \in \Omega$ . We define the first and the second fundamental forms by  $I = \langle dp, dp \rangle$ , and  $II = -\langle dn, dp \rangle$ , respectively. By using them, the Gauss curvature and the mean curvature are defined by  $K(x) = \det(I^{-1} II)$  and  $H(x) = \frac{1}{2} \text{tr}(I^{-1} II)$ , respectively.

**Proposition 5.3.** For a smooth surface  $p: \Omega \rightarrow \mathbb{R}^3$  with a unit normal vector field  $n$ , the Gauss curvature  $K$  satisfies  $\nabla_1 n(x) \times \nabla_2 n(x) = K(x)(\nabla_1 p(x) \times \nabla_2 p(x))$ , and the mean curvature  $H$  satisfies  $\frac{d}{dt} A(x, t)|_{t=0} = -H(x)A(x)$ , where  $A(x)$  is the area element of  $p$  and  $A(x, t)$  is the one of  $p + tn$ .

To define curvatures for trivalent discrete surfaces which are an analogue of Definition 5.2, it may be suffice to define the covariant derivative and the unit normal vector at each vertex of trivalent discrete surfaces, and we should prove that curvatures for trivalent discrete surfaces satisfy similar properties of Proposition 5.3.

**Definition 5.4 (Kotani–Naito–Omori [16]).** Let  $\Phi(X)$  be a trivalent discrete surface,  $\mathbf{x} \in \Phi(X)$ , and  $\mathbf{x}_1, \mathbf{x}_2, \mathbf{x}_3$  its adjacency vertices. We define the unit normal vector at  $\mathbf{x}$  as the normal vector of the plane through  $\mathbf{e}_1, \mathbf{e}_2, \mathbf{e}_3$  (see Fig. 5.1), that is,

$$n(\mathbf{x}) = \frac{(\mathbf{e}_2 - \mathbf{e}_1) \times (\mathbf{e}_3 - \mathbf{e}_1)}{|(\mathbf{e}_2 - \mathbf{e}_1) \times (\mathbf{e}_3 - \mathbf{e}_1)|} = \frac{\mathbf{e}_1 \times \mathbf{e}_2 + \mathbf{e}_2 \times \mathbf{e}_3 + \mathbf{e}_3 \times \mathbf{e}_1}{|\mathbf{e}_1 \times \mathbf{e}_2 + \mathbf{e}_2 \times \mathbf{e}_3 + \mathbf{e}_3 \times \mathbf{e}_1|},$$

and the covariant derivative as

$$\nabla_e \mathbf{x} = \text{Proj}(e) = e - \langle e, n(\mathbf{x}) \rangle n(\mathbf{x}), \quad e \in E_x,$$

where  $\mathbf{e}_i = \mathbf{x}_i - \mathbf{x}$ .

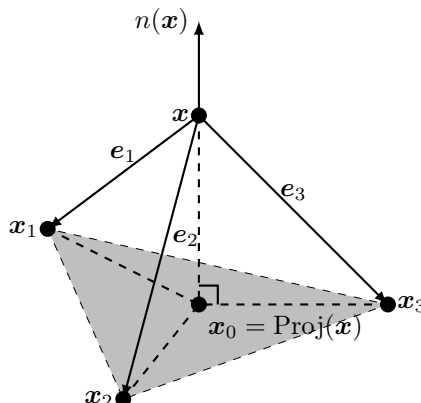


Figure 5.1: The unit normal vector for trivalent discrete surfaces. The area of the triangle filled in gray is the local area at  $\mathbf{x}$ .

**Definition 5.5** (Kotani–Naito–Omori [16]). Let  $X$  be a trivalent discrete surface and  $\mathbf{x}$  be a vertex of  $X$ . We define the first and the second fundamental forms by

$$\begin{aligned} \mathbf{I}(\mathbf{x}) &= \begin{pmatrix} \langle \mathbf{e}_2 - \mathbf{e}_1, \mathbf{e}_2 - \mathbf{e}_1 \rangle & \langle \mathbf{e}_2 - \mathbf{e}_1, \mathbf{e}_3 - \mathbf{e}_1 \rangle \\ \langle \mathbf{e}_3 - \mathbf{e}_1, \mathbf{e}_2 - \mathbf{e}_1 \rangle & \langle \mathbf{e}_3 - \mathbf{e}_1, \mathbf{e}_3 - \mathbf{e}_1 \rangle \end{pmatrix}, \\ \mathbf{II}(\mathbf{x}) &= - \begin{pmatrix} \langle \mathbf{e}_2 - \mathbf{e}_1, n_2 - n_1 \rangle & \langle \mathbf{e}_2 - \mathbf{e}_1, n_3 - n_1 \rangle \\ \langle \mathbf{e}_3 - \mathbf{e}_1, n_2 - n_1 \rangle & \langle \mathbf{e}_3 - \mathbf{e}_1, n_3 - n_1 \rangle \end{pmatrix}, \end{aligned}$$

and we define the Gauss curvature and the mean curvature at  $\mathbf{x}$  by

$$\begin{aligned} K(\mathbf{x}) &= \det(\mathbf{I}(\mathbf{x})^{-1} \mathbf{II}(\mathbf{x})), \\ H(\mathbf{x}) &= \frac{1}{2} \operatorname{tr}(\mathbf{I}(\mathbf{x})^{-1} \mathbf{II}(\mathbf{x})). \end{aligned}$$

Then, we obtain the following properties for curvatures of trivalent discrete surfaces.

**Theorem 5.6** (Kotani–Naito–Omori [16]). *For a trivalent discrete surface  $\Phi$ , the Gauss curvature  $K$  satisfies  $\nabla_i n(\mathbf{x}) \times \nabla_j n(\mathbf{x}) = K(\mathbf{x})(\mathbf{e}_i \times \mathbf{e}_j)$ , where  $\nabla_i = \nabla_{\mathbf{e}_i}$ , and the mean curvature  $H$  satisfies  $\frac{d}{dt} \Big|_{t=0} \mathcal{A}(\Phi + tn) = -2 \sum_{x \in V} H(\mathbf{x}) A(\mathbf{x})$ , where  $A(\mathbf{x}) = \mathbf{e}_1 \times \mathbf{e}_2 + \mathbf{e}_2 \times \mathbf{e}_3 + \mathbf{e}_3 \times \mathbf{e}_1$  is the local area at  $\mathbf{x}$  and  $\mathcal{A}(\Phi) = \sum_{x \in V} A(\mathbf{x})$  is the total area.*

**Remark 5.7.** Unfortunately, the second fundamental form  $\mathbf{II}$  of trivalent discrete surfaces is not symmetric in general.

**Theorem 5.8** (Kotani–Naito–Omori [16]). *Trivalent discrete surface  $\Phi$  is called **minimal** if and only if  $H(\mathbf{x}) = 0$ , which is expressed by the system of linear equation*

$$\nabla_{\mathbf{e}_2 - \mathbf{e}_3} n \times \nabla_{\mathbf{e}_1} \Phi + \nabla_{\mathbf{e}_3 - \mathbf{e}_1} n \times \nabla_{\mathbf{e}_2} \Phi + \nabla_{\mathbf{e}_1 - \mathbf{e}_2} n \times \nabla_{\mathbf{e}_3} \Phi = 0.$$

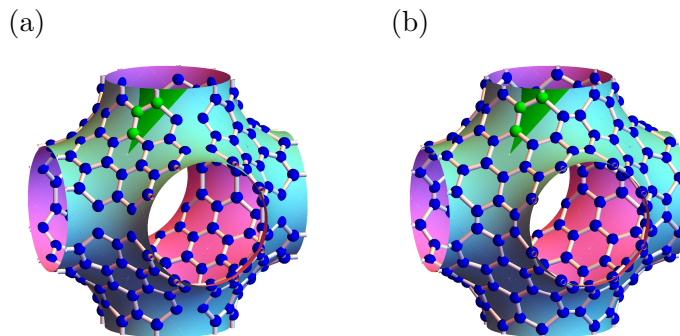


Figure 5.2: (a) Mackay–Terrones' structure (standard realization), (b) minimal realization of the same structure (Kotani–Naito–Omori [16]).

**Proposition 5.9** (Kotani–Naito–Omori [16]). *If a trivalent discrete surface is a plane graph, then  $K \equiv 0$ ,  $H \equiv 0$ . Here, a graph is called plane, if it is drawn in a plane without self-intersection. If a trivalent discrete surface satisfies  $\mathbf{x} = rn(\mathbf{x})$  for any  $x \in V$ , then  $K \equiv 1/r^2$ ,  $H \equiv -1/r$ .*

We call a surface satisfying the  $\mathbf{x} = rn(\mathbf{x})$  *sphere shaped*. Regular polyhedra and semi-regular polyhedra (including  $C_{60}$ ) are sphere shaped.

**Proposition 5.10** (Kotani–Naito–Omori [16]). *Let  $\text{CNT}(\lambda, \mathbf{c})$  be a SWNT with the chiral index  $\mathbf{c} = (c_1, c_2)$  and the scale factor  $\lambda$ , that is,  $(x, y) \mapsto (r(\lambda, \mathbf{c}) \cos(x/r(\lambda, \mathbf{c})), r(\lambda, \mathbf{c}) \sin(x/r(\lambda, \mathbf{c})), y)$ . Then the Gauss curvature and the mean curvature of  $\text{CNT}(\lambda, \mathbf{c})$  are*

$$K(\lambda, \mathbf{c}) = \frac{4m_z(\mathbf{c})^2(m_x(\mathbf{c})^2 + m_y(\mathbf{c})^2)}{3r(\lambda, \mathbf{c})^2(m_x(\mathbf{c})^2 + m_y(\mathbf{c})^2 + (4/3)m_z(\mathbf{c})^2)^2},$$

$$H(\lambda, \mathbf{c}) = -\frac{m_x(\mathbf{c})}{2r(\lambda, \mathbf{c})} \cdot \frac{m_x(\mathbf{c})^2 + m_y(\mathbf{c})^2 + (8/3)m_z(\mathbf{c})^2}{(m_x(\mathbf{c})^2 + m_y(\mathbf{c})^2 + (4/3)m_z(\mathbf{c})^2)^{3/2}},$$

where  $m_\alpha(\mathbf{c})$  is a quantity defined from the chiral index. In particular,  $c_1 = c_2$ , then  $m_z(\mathbf{c}) = 0$ , and

$$K(\lambda, \mathbf{c}) = 0, \quad H(\lambda, \mathbf{c}) = -\frac{1}{2r(\lambda, \mathbf{c})} \cos \frac{C_1}{2}.$$

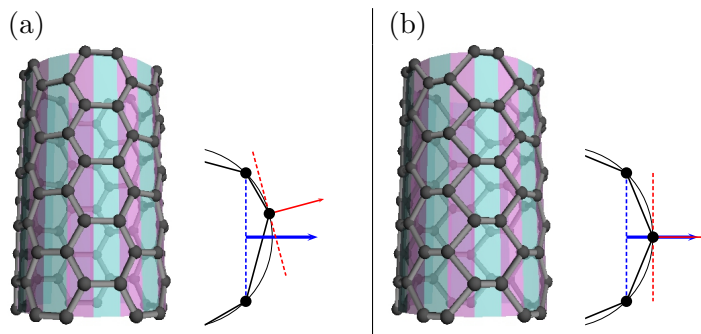


Figure 5.3: (a)  $\text{CNT}(\lambda, \mathbf{c})$  satisfies  $H \neq 1/r$ , whose normal vectors are not parallel to normal vectors of the underlying cylinder. (b) small change of  $\text{CNT}(\lambda, \mathbf{c})$  satisfies  $H \equiv 1/r$ , whose normal vectors are parallel to normal vectors of the underlying cylinder (Kotani–Naito–Omori [16]).

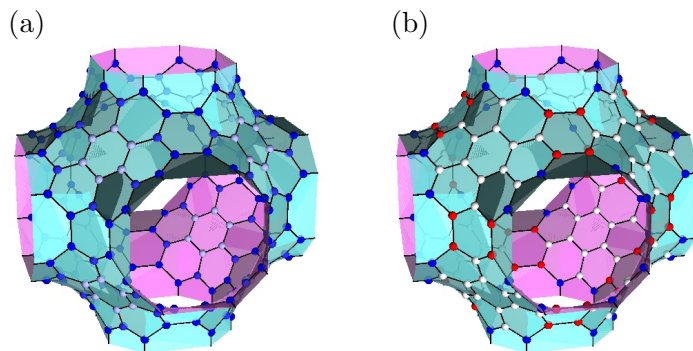


Figure 5.4: (a) The Gauss curvatures of Mackay–Terrones' structure, (b) the mean curvatures of Mackay–Terrones' structure. By our definition of curvatures, Mackay–Terrones' structure is *pointwise* negatively curved. Blue (red) vertices are negatively (positively) curved, and color densities express relative absolute values of curvatures (Kotani–Naito–Omori [16]).

**Remark 5.11.** Curvatures of  $K_4$  structure satisfy  $K > 0$  and  $H \equiv 0$ . In the case of smooth surfaces, the mean curvature  $H \equiv 0$  then the Gauss curvature  $K \leq 0$ , since the second fundamental form  $\text{II}$  is symmetric. On the other hand, in our discrete case,  $\text{II}$  is not symmetric, and thus  $H \equiv 0$  does not imply  $K \leq 0$ ,

## 5.2 Further problems

In [16], we discuss a convergence of sequence of “subdivision” of a trivalent discrete surface. In our context, there are no underlying continuous object, and trivalent discrete surfaces are essentially discrete object. For example, Mackay–Terrones’ structure is constructed by Schwarz P surface as model, but there are no relations between the structure and the surface itself. We would find a “limit” of a sequence of trivalent discrete surfaces, and make a relationship a trivalent discrete surface and a continuous surface.

To discuss a convergence theory of trivalent discrete surfaces, we should consider how to subdivide a trivalent graph, and how to realize the subdivided graph. Goldberg–Coxeter subdivision for trivalent graphs defined by Dutour–Deza [7, 8] is the good definition to subdivide a trivalent graph (see also Goldberg [11] and Omori–Naito–Tate [31]). Kotani–Naito–Omori [16], Tao [41], and Kotani–Naito–Tao [17] discuss convergences of sequences of trivalent discrete surfaces.

On the other hand, eigenvalues of the Laplacian of graphs are one of the main objects in discrete geometric analysis (see for example [4, 12, 22]). Eigenvalues of the Laplacian of graphs are also interest from physical and chemical view points (see also Section A.2). Some properties of eigenvalues of Laplacians of Goldberg–Coxeter constructions of trivalent graphs are discussed in Omori–Naito–Tate [31].

## A Appendix

### A.1 Space groups in $\mathbb{R}^2$ and $\mathbb{R}^3$

**Definition A.1.** A discrete finite subgroup  $P$  of  $O(d)$  is called a *point group* of  $\mathbb{R}^d$ , and a subgroup  $\Gamma$  of Euclidean motion group of  $\mathbb{R}^d$  is called a *space group* of  $\mathbb{R}^d$ , if  $\Gamma$  is discrete subgroup and  $\Gamma \cap T \cong \mathbb{Z}^d$ , where  $T$  is the group of parallel transformations in  $\mathbb{R}^d$ .

A 2-dimensional point group  $P$  is extended to a space group, if and only if  $P$  is 3-, 4-, or 6-fold symmetry, that is to say,  $P$  is one of  $C_1, C_2, C_3, C_4, C_6, D_1, D_2, D_3, D_4$ , and  $D_6$ . Here,  $C_n$  is the  $n$ -fold rotation group ( $\cong \mathbb{Z}_n$  cyclic group), and  $D_n$  is the  $n$ -fold rotation and reflection group (dihedral group).

It is a very famous old result that the number of 2-dimensional space groups is 17. 2-dimensional space groups may contain parallel transformations, 2-, 3-, or 6-folds rotations with respect to a point, and glide reflections with respect to a line. Here, a glide reflection is the composition of a reflection and a parallel transformation.

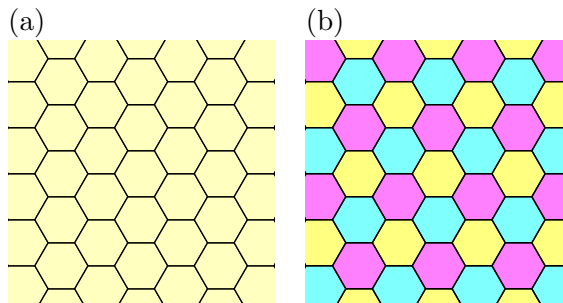


Figure A.1: Space groups of (a) and (b) are  $P6m$  and  $P3m1$ . Since  $P3m1$  is a subgroup of  $P6m$ , we can say that the figure (a) has higher symmetry than figure (b).

3-dimensional point groups are one of  $C_n, C_{nv}, C_{nh}, D_n, D_{nv}, D_{nh}, S_{2n}, T, T_d, T_h, O, O_h, I$ , and  $I_h$ . Here,  $C_{nv}$  ( $D_{nv}$ ) and  $C_{nh}$  ( $D_{nh}$ ) are  $C_n$  ( $D_n$ ) with additional mirror plane perpendicular

(parallel) to the axis to rotation, respectively, and  $S_{2n}$  is  $2n$ -fold rotation and reflection axis. Group  $T$ ,  $O$ , and  $I$  are well-known as polyhedral groups,  $T_d$  is  $T$  with improper rotations,  $T_h$ ,  $O_h$ , and  $I_h$  are  $T$ ,  $O$ , and  $I$  with reflections, respectively.

A 3-dimensional point group  $P$  extends a space group, if and only if  $P$  is 3-, 4-, or 6-fold symmetry, That is to say  $P$  is one of  $C_n$ ,  $C_{nv}$ ,  $C_{nh}$ ,  $D_n$ ,  $D_{nh}$ , and  $D_{nv}$ , ( $n = 1, 2, 3, 4, 6$ ).

It is also a famous old result that number of 3-dimensional space groups is 230. 3-dimensional space groups may contain parallel transformations, 2-, 3-, or 6-folds rotations with respect to a point, reflections/glide reflections with respect to a line, and improper rotation. Here a improper rotation is product with rotation and reflection with respect to a line perpendicular to rotation axis.

The space group of diamond crystals is  $Fd\bar{3}m$ , where  $F$ ,  $d$ ,  $\bar{3}$ , and  $m$  mean that ‘‘Face-centered cubic’’ structure, the group contains a glide reflection, the group contains 3 improper rotations, and the group contains a reflection, respectively.

## A.2 Electronic properties of carbon structures

States of electrons of atoms, molecules, and solids follow the Schrödinger equation

$$-\Delta\psi + V\psi = E\psi, \quad \text{in } \mathbb{R}^3, \quad (\text{A.1})$$

where  $V$  is a potential and  $E$  is the energy of an electron. In cases of crystal structures, the state  $\psi$  of electrons and the potential  $V$  are periodic, and hence taking the Fourier transformation of (A.1), we obtain

$$\widehat{H}\widehat{\psi}(\xi) = E(\xi)\widehat{\psi}(\xi), \quad (\text{A.2})$$

where  $H = -\Delta + V$ . The dispersive relation  $\xi \mapsto E(\xi)$  represents energies of electrons with the wave number  $\xi$  in a crystal.

As an example, we consider electronic states of graphenes. Considering  $\pi$ -electrons in graphenes, we obtain eigenvalues of  $\widehat{H}$ ,

$$E(\xi) = \pm\sqrt{3 + 2\cos(\xi_1) + 2\cos(\xi_2) + 2\cos(\xi_1 - \xi_2)}. \quad (\text{A.3})$$

As shown in Fig. A.2, the lower band (valence band) and the upper band (conductor band) attache at  $K$  and  $K'$  points with the Fermi energy (zero energy), and hence graphenes are conductor (metal). Moreover, at  $K$  and  $K'$  points, both bands have cone singularities. Such points are called *Dirac points*. On Dirac points, effective masses of electrons is zero, which are very important properties in solid state physics. Note that crystals whose conductor bands and valence bands intersects are called metals or conductors, and crystals whose conductor/valence bands does not intersects but its gap less than about 1 eV are called semi-conductors.

This calculation, which is called the *tight-binding approximation*, includes only interaction arise from nearest atoms with respect to each atom. Hence, the tight-binding approximations is based on graph theories, actions of an abelian group, and the Fourier transformations, mathematically.

To calculate of electronic states of  $C_{60}$ , we cannot apply the tight-binding approximation, since  $C_{60}$  is not a crystal structure, but a molecule structure. The *Hückel method* admits calculations of orbitals in hydrocarbon molecules, and is also based on graph theories. Let  $X = (V, E)$  be the graph of a molecule structure, that is,  $V$  are set of carbon atoms, and  $E$  are set of covalent bonds between carbon atoms. Eigenvectors  $\psi$  of the adjacency matrix  $A$  of  $X$  are molecular orbitals of electrons, and their eigenvalues  $\lambda$  are energies of orbitals.

**Example A.2.** Consider benzene molecules ( $C_6H_6$ ), which contains six carbon atoms, and whose graph is  $C_6$  (the cyclic graph with six vertices), and number of electrons of  $\pi$ -orbitals (not

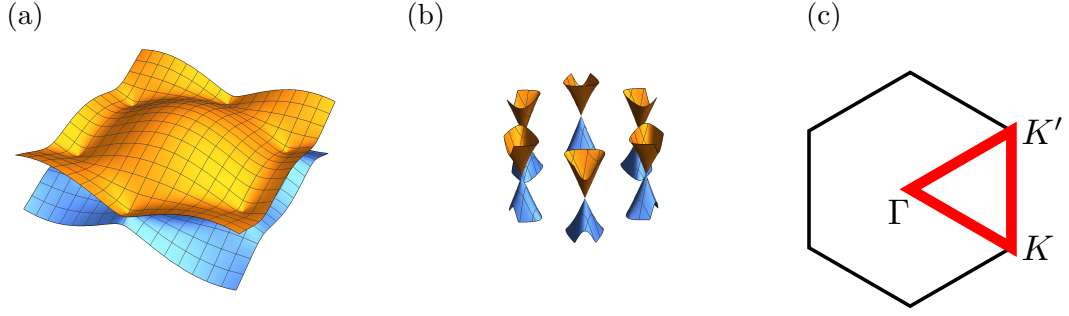


Figure A.2: (a)  $E(\xi)$  of graphenes (band structure), (b) closed up  $E(\xi)$  near  $K$  and  $K'$  points. (c) highly-symmetric points in the Fourier space.

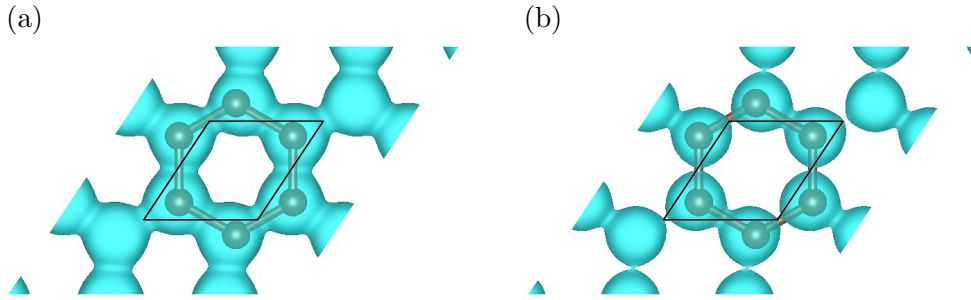


Figure A.3: Iso-surfaces of density of electrons in graphenes by using density functional theory (DFT). (a) probability 0.18, (b) probability 0.30.

using covalent bonds) is also six. Eigenvalues of adjacency matrix of  $C_6$  are  $\{2, 1, 1, -1, -1, -2\}$ , and electrons in  $\pi$ -orbital occupy orbitals with energies  $\{-1, -1, -2\}$  in the ground state, since each orbital can contain two electrons by Pauli's principle. We can write the wave function of the ground state as  $\psi = \sum_{i=1}^3 c_{ij} \chi_j$  by using eigenvectors  $\{\chi_j\}_{j=1}^6$ , and we obtain  $\sum_{i=1}^3 c_{ij}^2 = 1/2$ . This means that  $\pi$ -electrons have equal distributions on each carbon atom.

By using similar calculations, we also obtain  $\pi$ -electrons have equal distributions on each carbon atom on  $C_{60}$  (see also Fig. A.4).

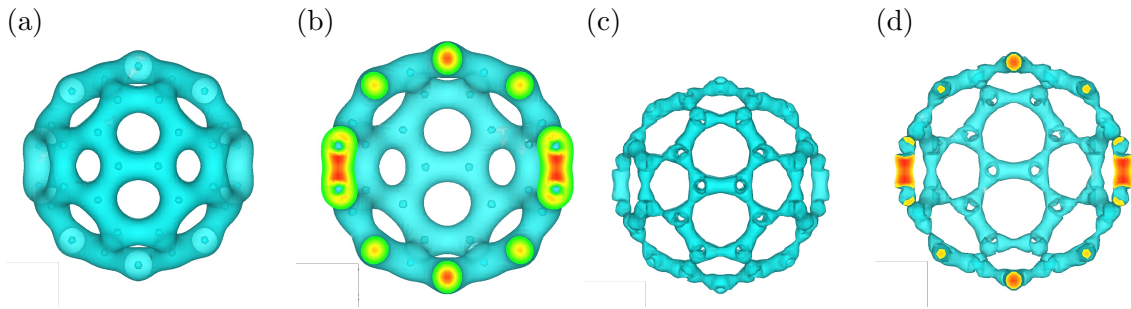


Figure A.4: Iso-surface of distributions of electrons of  $C_{60}$  by DFT. (a) probability 0.15, (b) its cut-model, (c) probability 0.25, (d) its cut-model.

### A.3 Carbon nanotubes from geometric view points

Carbon nanotubes are carbon allotropes, whose carbon atoms chemically bind with other three atoms with  $sp^2$ -orbitals, and they are graphenes rolled up in cylinders. There are many types

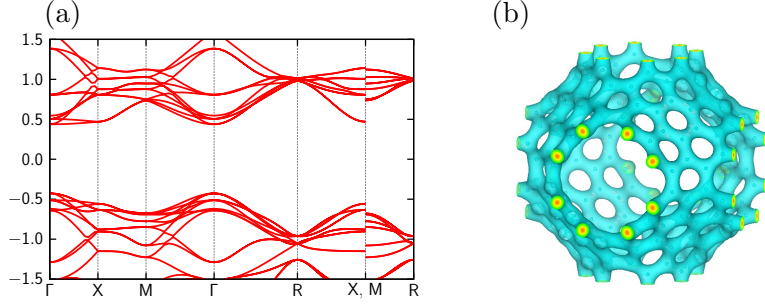


Figure A.5: DFT calculation result for Mackay-Terrones' structure. (a) electronic state, band gap is about 1 eV, and hence Mackay-Terrones' structure is semi-conductor, (b) iso-surface of density of electrons ( $p = 0.15$ ).

of carbon nanotubes. However, in this section, we only consider single wall nanotubes (SWNT). SWNTs have a parameter (*chiral index*)  $\mathbf{c} = (c_1, c_2)$ , which is defined as follows.

Choose a vertex of a regular hexagonal lattice (a graphene) as an origin  $(0, 0)$ , the select fundamental piece, whose vertices are  $\{\mathbf{v}_i\}_{i=0}^3$  of a regular hexagonal lattice (A.4), and translation vectors as (A.5):

$$\mathbf{v}_0 = (0, 0), \quad \mathbf{v}_1 = (0, -1), \quad \mathbf{v}_2 = (1/2, \sqrt{3}/2), \quad \mathbf{v}_3 = (-1/2, \sqrt{3}/2), \quad (\text{A.4})$$

$$\mathbf{a}_1 = (\sqrt{3}, 0), \quad \mathbf{a}_2 = (1/2, -\sqrt{3}/2). \quad (\text{A.5})$$

Select  $(c_1, c_2)$  with  $c_1 \in \mathbb{N}_{>0}$  and  $c_2 \in \mathbb{N}_{\geq 0}$ , and set  $\mathbf{c} = c_1\mathbf{a}_1 + c_2\mathbf{a}_2$ , we call  $\mathbf{c}$  a *chiral vector* (or chiral index) of SWNT. On the other hand,  $\mathbf{t} = (1/\text{gcd}(c_1, c_2))((c_1 + 2c_2)\mathbf{a}_1 - (2c_1 + c_2)\mathbf{a}_2)$ , which is called a lattice vector, satisfies  $\langle \mathbf{c}, \mathbf{t} \rangle = 0$ .

A SWNT with the chiral index  $\mathbf{c}$  is the structure identifying  $\mathbf{0}$  and  $\mathbf{c}$ , along the line between  $\mathbf{0}$  and  $\mathbf{t}$ . Note that the fundamental region of the SWNT with the chiral index  $\mathbf{c}$  is the rectangle with vertices  $\mathbf{0}$ ,  $\mathbf{t}$ ,  $\mathbf{t} + \mathbf{c}$ , and  $\mathbf{c}$ . The diameter of a SWNT with chiral index  $\mathbf{c} = (c_1, c_2)$  is  $L = \sqrt{c_1^2 + c_1c_2 + c_2^2}$ .

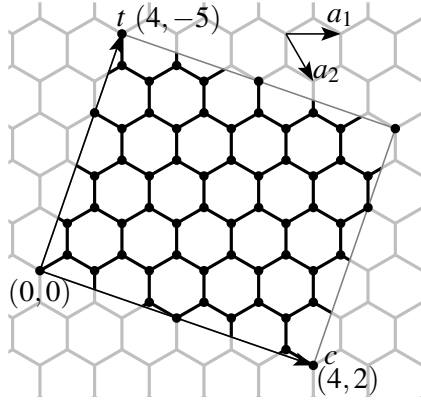


Figure A.6: Construction of a SWNT from a regular hexagonal lattice

Recently, there are several research composing a SWNT with short length using organic chemistry (see for example [26]), and hence an index measuring the length of SWNTs is needed. Matsuno–Naito–Hitosugi–Sato–Kotani–Isobe propose such an index, which is called the *length index* of SWNT [26]:

$$\frac{\sqrt{3}|c_1(a_1 - b_1) - c_2(a_2 - b_1)|}{2\sqrt{c_1^2 + c_1c_2 + c_2^2}}, \quad \text{with edge atoms coordinates } (a_1, b_1) \text{ and } (a_2, b_1). \quad (\text{A.6})$$



The index (A.6) measures how many benzene rings (hexagons) are in the length direction.

SWNTs with  $c_1 = c_2$  are called *zigzag type*,  $c_2 = 0$  are called *armchair type*, and otherwise are called *chiral type*. These names come from shape of edges of SWNTs (see Fig. A.7).

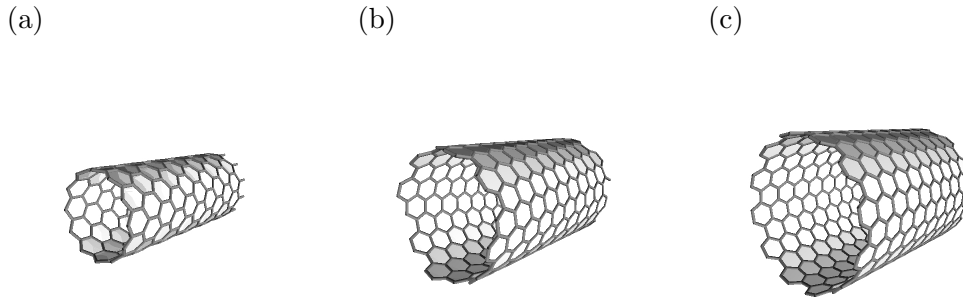


Figure A.7: (a) A zigzag type ( $\mathbf{c} = (12, 0)$ ), (b) a chiral type ( $\mathbf{c} = (12, 8)$ ), (c) an armchair type ( $\mathbf{c} = (12, 12)$ ).

Electronic properties of SWNTs are also geometric. The following result is well-known, and is obtained by tight binding approximations. If  $c_1 \equiv c_2 \pmod{3}$ , then SWNTs with  $\mathbf{c} = (c_1, c_2)$  are metallic, if not, then such SWNTs are semi-conductors.

## Acknowledgement

This note is based on lectures in “Introductory Workshop on Discrete Differential Geometry” at Korea University on January 21–24, 2019. The author greatly thanks to organizers of the workshop, and hospitality of Korea University. The author thanks to Mr. Tomoya NAITO (Department of Physics, The University of Tokyo), who calculates Figures A.3, A.4, and A.5 by Density Functional Theory by using OPENMX [23, 32, 33, 34] and read my manuscript and give the author valuable comments. The author also thanks to Professor Motoko KOTANI (AIMR, Tohoku University) and Dr. Shintaro AKAMINE (Graduate School of Mathematics, Nagoya University), who read my manuscript and give the author valuable comments. This work is partially supported by KAKENHI 17H06466.

## References

- [1] A. V. Aho, J. E. Hopcroft, and J. D. Ullman, *The Design and Analysis of Computer Algorithms*, Pearson, 1974.
- [2] The Australian National University, The EPINET Project. <http://epinet.anu.edu.au/>
- [3] J. A. Bondy and U. S. R. Murty, *Graph Theory*, Graduate Texts in Mathematics vol. 244, Springer, 2008.
- [4] D. Cvetković, P. Rowlinson, and S. Simić, *An Introduction to the Theory of Graph Spectra*, London Math. Soc., Student Texts vol. 75, 2010.
- [5] G. Davidoff, P. Sarnack, and A. Valette, *Elementary Number Theory, Group Theory, and Ramanujan Graphs*, London Math. Soc., Student Texts vol. 55, 2003.
- [6] O. Delgado-Friedrichs and M. O’Keeffe, Identification of and symmetry computation for crystal nets. *Acta Crystallogr. A*, **59**, 351–360, (2003). doi:10.1107/S0108767303012017

- [7] M. Deza and M. Dutour Sikirić, *Geometry of chemical graphs: polycycles and two-faced maps*, volume 119 of *Encyclopedia of Mathematics and its Applications*. Cambridge University Press, Cambridge, 2008. doi:10.1017/CBO9780511721311
- [8] M. Dutour and M. Deza, Goldberg-Coxeter construction for 3- and 4-valent plane graphs, *Electron. J. Combin.*, **11**, Research Paper 20, 49, (2004).  
http://www.combinatorics.org/Volume\_11/Abstracts/v11i1r20.html
- [9] J. Eells and J. H. Sampson, Harmonic mappings of Riemannian manifolds, *Amer. J. Math.*, **86**, 109–160, (1964). http://www.jstor.org/stable/2373037
- [10] D. Fujita, Y. Ueda, S. Sato, N. Mizuno, T. Kumasaka, and M. Fujita, Self-assembly of tetravalent Goldberg polyhedra from 144 small components, *Nature*, **540**, 563, (2016). doi:10.1038/nature20771
- [11] M. Goldberg, A class of multi-symmetric polyhedra, *Tohoku Math. J.*, First Series, **43**, 104–108, (1937).  
https://www.jstage.jst.go.jp/article/tmj1911/43/0/43\_0\_104/\_pdf/-char/en
- [12] Yu. Higuchi, and T. Shirai, Some spectral and geometric properties for infinite graphs, *Contemp. Math.*, **347**, 29–56, (2004). doi:10.1090/conm/347/06265
- [13] M. Itoh, M. Kotani, H. Naito, T. Sunada, Y. Kawazoe, and T. Adschiri, New metallic carbon crystal, *Phys. Rev. Lett.*, **102**, 055703, (2009). doi:10.1103/PhysRevLett.102.055703
- [14] T. Kajigaya and R. Tanaka, Uniformizing surfaces via discrete harmonic maps, arXiv:1905.05427.
- [15] K. Kawasumi, Q. Zhang, Y. Segawa, L. T. Scott and K. Itami, A grossly warped nanographene and the consequences of multiple odd-membered-ring defects, *Nature Chemistry*, **5**, 739–744 (2013). doi:10.1038/NCHEM.1704
- [16] M. Kotani, H. Naito, and T. Omori, A discrete surface theory, *Comput. Aided Geom. Design*, **58**, 24–54, (2017). doi:10.1016/j.cagd.2017.09.002
- [17] M. Kotani, H. Naito, and C. Tao, Construction of continuum from a discrete surface by its iterated subdivisions, arXiv:1806.03531.
- [18] M. Kotani and T. Sunada, Albanese maps and off diagonal long time asymptotics for the heat kernel, *Comm. Math. Phys.*, **209**, 633–670, (2000). doi:10.1007/s002200050033
- [19] M. Kotani and T. Sunada. A central limit theorem for the simple random walk on a crystal lattice, Proceedings of the Second ISAAC Newton Congress, vol. 1, 1–6, 2000, Springer. doi:10.1007/978-1-4613-0269-8\_1
- [20] M. Kotani and T. Sunada, Jacobian tori associated with a finite graph and its abelian covering graphs, *Adv. in Appl. Math.*, **24**, 89–110, (2000). doi:10.1006/aama.1999.0672
- [21] M. Kotani and T. Sunada, Standard realizations of crystal lattices via harmonic maps, *Trans. Amer. Math. Soc.*, **353**, 1–20, (2001). doi:10.1090/S0002-9947-00-02632-5
- [22] M. Kotani and T. Sunada, Spectral geometry of crystal lattices, *Contemp. Math.*, **338**, 271–305, (2003). doi:10.1090/conm/338/06077
- [23] K. Lejaeghere, *et al.*, Reproducibility in density functional theory calculations of solids, *Science*, **351**, aad3000, (2016). doi:10.1126/science.aad3000

- [24] T. Lenosky, X. Gonze, M. Teter, and V. Elser, Energetics of negatively curved graphitic carbon, *Nature*, **355**, 333–335, (1992). doi:10.1038/355333a0
- [25] A. Mackay and H. Terrones, Diamond from graphite, *Nature*, **352**, 762, (1991). doi:10.1038/352762a0
- [26] T. Matsuno, H. Naito, S. Hitosugi, S. Sato, M. Kotani, and H. Isobe, Geometric measures of finite carbon nanotube molecules: A proposal for length index and filling indexes, *Pure Appl. Chem.*, **86**, 489–495 (2014). doi:10.1515/pac-2014-5006
- [27] A. Mizuno, Y. Shuku, M. M. Matsushita, M. Tsuchiizu, Y. Hara, N. Wada, Y. Shimizu, and K. Awaga, 3D spin-liquid state in an organic hyperkagome lattice of mott dimers, *Phys. Rev. Lett.*, **119**, 057201 (2017). doi:10.1103/PhysRevLett.119.057201
- [28] H. Naito, Visualization of standard realized crystal lattices, *Contemp. Math.*, **484**, 153–164, (2009). doi:10.1090/conm/484/09472
- [29] H. Naito, Construction of negatively curved carbon crystals via standard realizations, *Springer Proc. Math. Stat.*, **166**, 83–100, (2016). doi:10.1007/978-4-431-56104-0\_5
- [30] M. O’Keeffe and B. G. Hyde, Plane nets in crystal chemistry, *Philos. Trans. R. Soc. A*, **295**, 553-618, (1980). doi:10.1098/rsta.1980.0150
- [31] T. Omori, H. Naito, and T. Tate, Eigenvalues of the Laplacian on the Goldberg-Coxeter constructions for 3- and 4-valent graphs, *Electron. J. Combin.*, **26(3)**, (2019), #P3.7. <https://www.combinatorics.org/ojs/index.php/eljc/article/view/v26i3p7>
- [32] T. Ozaki, Variationally optimized atomic orbitals for large-scale electronic structures, *Phys. Rev. B*, **67**, 155108, (2003). doi:10.1103/PhysRevB.67.155108
- [33] T. Ozaki and H. Kino, Numerical atomic basis orbitals from H to Kr, *Phys. Rev. B*, **69**, 195113, (2004). doi:10.1103/PhysRevB.69.195113
- [34] T. Ozaki and H. Kino, Efficient projector expansion for the *ab initio* LCAO method, *Phys. Rev. B*, **72**, 045121, (2005). doi:10.1103/PhysRevB.72.045121
- [35] K. B. Petersen and M. S. Pertersen, *The Matrix Cookbook*, <https://www.math.uwaterloo.ca/~hwolkowi/matrixcookbook.pdf>
- [36] L. M. Singer and J. A. Thorpe, *Lecture Notes on Elementary Topology and Geometry*, Springer, 1967. <https://www.springer.com/gp/book/9780387902029>
- [37] T. Sunada, Crystals that nature might miss creating, *Notices Amer. Math. Soc.*, **55**, 208–215, (2008). <http://www.ams.org/notices/200802/tx080200208p.pdf>  
T. Sunada, Correction: “Crystals that nature might miss creating”, *Notices Amer. Math. Soc.*, **55**, 343, (2008). <https://www.ams.org/journals/notices/200803/tx080300342p.pdf>
- [38] T. Sunada. Lecture on topological crystallography, *Jpn. J. Math.*, **7**, 1–39, (2012). doi:10.1007/s11537-012-1144-4
- [39] T. Sunada, *Topological crystallography*, vol. 6 of *Surveys and Tutorials in the Applied Mathematical Sciences*. Springer, Tokyo, 2013. doi:10.1007/978-4-431-54177-6

- [40] M. Tagami, Y. Liang, H. Naito, Y. Kawazoe, and M. Kotani, Negatively curved cubic carbon crystals with octahedral symmetry, *Carbon*, **76**, 266–274, (2014). doi:10.1016/j.carbon.2014.04.077
- [41] C. Tao, A construction of converging Goldberg-Coxeter subdivisions of a discrete surface, preprint, (2018).
- [42] M. Tsuchiizu, Three dimensional higher-spin Dirac and Weyl dispersions in strongly isotropic  $K_4$  crystal, *Phys. Rev B*, **94**, 195426, (2016). doi:10.1103/PhysRevB.94.195426
- [43] S. Zhang, J. Zhou, Q. Wang, X. Chen, Y. Kawazoe, and P. Jena, Penta-graphene: A new carbon allotrope, *Proc. Nat. Acad. Sci.*, **112** 2372–2377, (2015). doi:10.1073/pnas.1416591112